HHS Public Access

Author manuscript

Pflugers Arch. Author manuscript; available in PMC 2016 October 01.

Published in final edited form as:

Pflugers Arch. 2015 October ; 467(10): 2193–2218. doi:10.1007/s00424-014-1674-0.

Impedance analysis of GPCR-mediated changes in endothelial barrier function: overview, and fundamental considerations for stable and reproducible measurements

Judith A. Stolwijk[1,2], **Khalid Matrougui**[3], **Christian W. Renken**[2], and **Mohamed Trebak**[1,$]

[1]The SUNY College of Nanoscale Science and Engineering (CNSE), SUNY Polytechnic Institute; State University of New York, Albany, NY

[2]Applied BioPhysics Inc., Troy, NY

[3]Department of Physiological Sciences, East Virginia Medical School, Norfolk, VA.

Abstract

The past 20 years have seen significant growth in using impedance-based assays to understand the molecular underpinning of endothelial and epithelial barrier function in response to physiological agonists, pharmacological and toxicological compounds. Most studies on barrier function use G protein coupled receptor (GPCR) agonists which couple to fast and transient changes in barrier properties. The power of impedance based techniques such as Electric Cell-Substrate Impedance Sensing (ECIS) reside in its ability to detect minute changes in cell layer integrity label-free and in real-time ranging from seconds to days. We provide a comprehensive overview of the biophysical principles, applications and recent developments in impedance-based methodologies. Despite extensive application of impedance analysis in endothelial barrier research little attention has been paid to data analysis and critical experimental variables, which are both essential for signal stability and reproducibility. We describe the rationale behind common ECIS data presentation and interpretation and illustrate practical guidelines to improve signal intensity by adapting technical parameters such as electrode layout, monitoring frequency or parameter (resistance versus impedance magnitude). Moreover, we discuss the impact of experimental parameters, including cell source, liquid handling and agonist preparation on signal intensity and kinetics. Our discussions are supported by experimental data obtained from human microvascular endothelial cells challenged with three GPCR agonists, thrombin, histamine and Sphingosine-1-Phosphate.

Keywords

ECIS; Endothelial Cells; Barrier function; Impedance; Resistance; TEER

[$]**Correspondence**: Mohamed Trebak, PhD. State University of New York College Polytechnic Institute, 257 Fuller Rd. Albany, NY 12203; USA. Phone: (518) 437-8639, Fax (518) 437-8687, mtrebak@albany.edu.

Disclosures

Judith Stolwijk is partially supported by a postdoctoral fellowship from Applied Biophysics Inc.

1. Introduction

In vitro assays for studying the barrier function of endothelial cells isolated from either the peripheral circulation or the brain-blood barrier (BBB) have become a valuable tool in cardiovascular and neurovascular research. These *in vitro* measurements support and complement *in vivo* and whole tissue experiments and have led to a better understanding of vascular and neurovascular pathologies as well as endothelial development, repair, differentiation and intracellular signaling mechanisms.

Existing *in vitro* assays to study barrier function of cultured endothelial cells rely either on the passage of labeled tracer molecules or on the passage of electrical currents carried by ions across the endothelial cell layer [70,109,125]. The latter mode represents the basis for electrical resistance measurements across endothelial and epithelial cell layers. Since, from an electrical perspective, cells essentially behave like insulating particles with their membranes functioning as insulating dielectric shells, movement of ionic charge carriers across a cell layer is predominantly facilitated by the intercellular shunts. Especially, cell-cell junctions limit ionic movement across the intercellular cleft and this is accordingly reflected in a high transendothelial electrical resistance of the cell layer. To electrically measure ion mobility across endothelial cell layers, electrodes have to be introduced into the culture system [70,109,111]. The possible electrode arrangements are essentially determined by the nature of the cell culture growth substrate and will be discussed further below.

ECIS was invented in 1984 by Giaever and Keese as an alternative method to the use of microscopes to study cell behavior electrically [38]. In Electric Cell-Substrate Impedance Sensing (ECIS), the cells are grown onto the surface of substrate-integrated planar thin-film electrodes of an inert nobel metal (e.g. gold) or metal oxides (e.g. indium tin oxide: ITO). Weak sinusoidal alternating currents (4 mA/cm^2) with frequencies ranging from 10 Hz to 10^5 Hz are applied to the electrodes to measure the impedance of the system. Alterations in the degree of electrode coverage with cells change the system's impedance. More importantly, ECIS is sensitive to changes in cell morphology. Changes in morphology are essentially evoked by alterations in the architecture of the cell structural components such as the cytoskeleton and cell-cell and cell-substrate junctions, which are the major determinants of endothelial barrier function.

The proof of principle of ECIS in the study of endothelial barrier function was first documented in 1992 [102]. Bovine pulmonary microvascular endothelial cells were cultured on small circular thin film gold electrodes to study changes in endothelial barrier in response to thrombin stimulation. Real-time measurement of resistance at 4000 Hz upon thrombin stimulation showed an immediate drop and subsequent recovery to baseline values within approximately three hours, which reflected the transient collapse of endothelial barrier. This experiment documented for the first time that the decrease in endothelial electrical resistance as measured with ECIS essentially reflects thrombin-induced endothelial barrier disruption, as previously measured using filter-based permeability studies with ^{125}I-albumin [37,63]. In contrast to the use of ^{125}I-albumin, label-free ECIS provided a much better temporal resolution and further enabled measurements of barrier recovery subsequent to the transient barrier disruption caused by thrombin. Since then, ECIS has developed into a popular *in*

vitro standard technique for the study of vascular barrier function [114,125]. This was particularly important for studies aimed at recording the immediate response of the endothelial monolayer to stimulation with inflammatory mediators that temporarily disrupt barrier integrity, many of which signal through G-protein-coupled receptors (GPCRs). Furthermore, ECIS allows accurate monitoring of endothelial monolayer integrity in response to barrier-stabilizing mediators and also offers a standardized system to study the molecular signaling mechanisms that control changes in barrier function in response to various agonists and mediators.

In the late 90's, the interdigitated electrodes (IDEs) have been introduced for impedance-based cell Monitoring by Ehret et al. [31,32]; followed by the real-time cell electronic sensing (RT-CES) technology by Solly et al. in 2004 [92]. The IDEs technology has been incorporated in the Bionas biosensor to enable encompassing quantification of cell behavior (www.bionas-discovery.com). The RT-CES technology has been commercialized as the xCelligence system by Acea Biosystems and Roche (www.aceabio.com), which also found broad application in endothelial and epithelial barrier function studies [4,19,34,49,61,74,96].

Even though a significant amount of literature has been published in the endothelial field using commercial impedance systems, in principle, powerful impedance measurement setups can be built in-house. Requirements are an impedance analyzer and culture ware with an incorporated two-electrode layout, where at least one of the electrodes is substrate-integrated. All solid substrate based impedance techniques rely on the same basic principle. However, due to differences in electrode layout and size, the measurement system, data calculation, analysis and presentation providing all-encompassing guidelines that are applicable to the different systems is challenging. Therefore, this manuscript is predominantly focused on addressing endothelial barrier function studies using the ECIS® technique developed by Applied BioPhysics Inc. (www.biophysics.com). Nevertheless, most of the general guidelines contained herein can be translated to other impedimetric setups. And an understanding of the differences between available techniques is a prerequisite to exploit the experimental scope for assay improvement.

To support our points of discussion, we include typical ECIS response profiles of primary human dermal microvascular endothelial cells (HDMEC) in response to distinct barrier-modifying GPCR agonists, namely thrombin, histamine and S1P (Fig. 1). We use these examples to illustrate how certain experimental conditions influence the outcome of the experiment.

Thrombin, which causes a transient but drastic disruption of endothelial cell-cell junctions, is often used as a model agonist to study the intracellular signal transduction pathways and cytoskeleton-associated proteins involved in endothelial barrier regulation [66,109]. Pharmacological modulation or molecular manipulation (gene knockdown or knockout) of a signaling protein or pathway can affect thrombin-mediated disruption of the endothelial barrier in a protective or destabilizing manner. Such effects can be directly and continuously measured by ECIS as changes in the magnitude of resistance decrease and in the kinetics of barrier breakdown and recovery upon thrombin stimulation. Furthermore, depending on the type of agonist considered (e.g. thrombin, histamine or sphingosine-1-phosphate (S1P)), the

effects on endothelial barrier is different in terms of profile, magnitude, and kinetics (Fig. 1). While thrombin and histamine both lead to a disruption of the endothelial barrier, in the case of histamine this disruption is relatively less potent and display a faster recovery. By contrast, S1P has barrier enhancing effects [36,122]. The capabilities of either agonist to promote barrier disruption or stabilization depend greatly on the actual maturity of the cell layer. For instance, barrier disrupting agonists such as thrombin or histamine may fail to affect the endothelial layer resistance if the cell layer is not confluent or the cell-cell junctions are immature. In a similar manner, barrier stabilizing agonists such as S1P may have only marginal or no effect on the barrier if the cell layer is well-matured and has reached its maximal density of cell-cell junction proteins and structural stability. The expression of cell-cell junctions depends on various factors such as vascular bed origin, cell passage, cell density and cell culture parameters, including culture medium composition. Furthermore, when working with primary cells from varying donor tissue, genetic and epigenetic factors have to be considered. In this context, the well-appreciated and extremely high sensitivity of ECIS can lead to difficulties in reproducibility and signal stability. As inconsistencies in experimental conditions and biological variability are reflected in electrical impedance of the cell layer, highly variable results can be generated. This manuscript aims to provide basic technical background of ECIS and to supply guidelines for the setup of a successful endothelial barrier function experiment.

2. Overview of endothelial barrier function assays

ECIS is only one of various *in vitro* approaches that have been developed to investigate endothelial and epithelial barrier regulation. An overview of the different *in vitro* techniques available will help understand the advantages and limitations of ECIS compared to other methods. *In vitro* assays for studying barrier function on cultured endothelial cells can be grouped into filter-based methods and solid-substrate based methods (Fig. 2). These methods either measure permeability of cell layers towards (macro-) molecular compounds or use label-free electrical measurements that determine electrical resistance across the cell layer based on Ohm's law ($R=V/I$) as an indication of cell monolayer permeability.

2a Filter-based assays for Macromolecular Permeability

Cell culture on porous filters has been successfully used to study barrier function of endothelial and epithelial tissue over several decades (Fig. 2a, b). Cell culture on a porous substrate somewhat mimics the *in vivo* situation by creating two compartments separated by the cell layer. In these systems the upper compartment of the filter typically reflects the luminal side, while the lower compartment represents the abluminal side of the barrier forming tissue. One easy approach to study barrier properties, without the need for expensive equipment, is to quantify the permeation rate of a chromophore/fluorophore- or a radioisotope-labeled tracer compound (e.g. FITC-albumin, FITC-dextran, [^{13}C]-sucrose, [^{3}H]-inulin, [^{125}I]-albumin), which are well described in various current reviews [21,70,109,125] and will be briefly discussed for completeness (Fig. 2a). The tracer molecule is added to the upper compartment (luminal side) of the cell layer and the amount of molecules that cross the cell layer over time is detected in the lower compartment via optical (photometry, fluorometry) or radiometric techniques. The permeability coefficient

can then be calculated using the time required for the accumulation of the tracer molecule in the abluminal compartment. Using molecular tracers that vary in physicochemical properties, such as size or charge, enable determining the route of permeation across an epithelial or endothelial tissue and the molecular composition of the barrier. Different molecular weight dextrans for example show size dependend transport across the vascular wall, which pointed to the existence of two distinct transport routes – a paracellular pathway for ions (Na^+, Cl^- , Ca^{2+}, Mg^{2+}, HCO^-) and small hydrophilic molecules such as water, urea, glucose and small proteins (< 3 nm) and a transcellular route for most proteins and larger molecules [69,66]. Ion selective transport across endothelia and epithelia quantified by radiometry (^{22}Na, ^{45}Ca, ^{86}Rb) or colorimetric detection can provide good indications on the molecular composition of cell-cell junctional structures such as the contribution of ion-selective Claudins. These approaches are often used to study permeability and filtering properties of transport accross epithelia such as the renal epithelium [99,3,94]. Moreover, filter-based molecular transport assays are well-appreciated in the study of the blood brain barrier (BBB) and its interaction with possible drug candidates, as they can reveal information on drug permeability, toxicity or effect on efflux transporters [116].

Tracer molecule-based measurements using endothelial cell layers grown on porous filters are integral. This means that possible defects in the cell layer will contribute to the overall readout where they go typically undetected. Unless certain tracer compounds are used that are exclusively transported via the paracellular pathway, such as dextrans, sucrose and inulin, one cannot distinguish if the molecular tracer has passed the cell layer via the paracellular or transcellular route.

2b Solid substrate-based assays for Macromolecular Permeability

To solve limitations of filter-based solute permeability, solid substrate-based techniques have been developed more recently [30,67] (Fig. 2c). Tracer compounds are either collected at the abluminal side of the cell layer by diffusion into cuvette-like micropores [67] or immobilized on the culture substrate by biotin / avidin interactions [30] (Fig. 2c). For example, the cuvette-like micropores, which are significantly smaller than cells, allow collection of compounds that diffuse across a small portion of each cell with high spatial resolution [67]. Such high spatial resolution would potentially allow for determination of the relative fraction of compounds that enters the microcuvettes *via* either cell-cell junctions or the transcellular route. The detection of these relative fractions can be subsequently confirmed by confocal microscopy. Individual microcuvettes can reveal spatially-restricted single cell defects within the cell layer; such localized defects often compromise the accuracy of measurements in conventional filter assays.

Even though tracer molecule-based assays are straightforward in theory, these permeability studies are quite time consuming and the lack of automatization limits parallelization and temporal resolution. Limitations with the use of macromolecular tracer compounds also lie in the differences in physico-chemical properties of various tracer molecules. Size, polarity and charge of the tracer compound can influence the permeation efficiency and route significantly, which create a challenge for data interpretation. This is especially of concern when the molecular structures that promote the transport of tracers used are not yet

identified. Importantly, the concentration gradient across the cell layer drives the accumulation of tracer molecules into the lower compartment until equilibrium is reached. This fact combined with the low temporal resolution limits the level of detailed information obtained on the dynamics of permeability changes across cell layers. This means that molecule permeability measurements become particularly ineffective when applied to the study of the recovery phase of the cell monolayer's barrier properties subsequent to treatments that reversibly alter barrier function. Thus, fast dynamic and transient alterations in barrier integrity, as typically found under physiological stimulation of cell surface receptors might not be readily detectable and their molecular basis goes undetected.

2c Electrical Methods

To circumvent the use of macromolecular tracer compounds, electrical methods have been developed that rely on the permeability of endothelia towards small ionic species abundantly available in physiological cell media (mainly ions such as Na^+, Cl^- and HCO_3^-) and measured electrically (Fig. 2b, d). Since ionic mobility across the cell layer is driven by an externally applied electric field instead of a concentration gradient, electrical methods are not limited by the extinction of a molecule gradient and are not only sensitive to barrier-disrupting, but also barrier-restoring processes. Moreover, measuring overall electrical conductivity bypasses ion selectivity across barriers with well-established and ion selective tight junctional structures [99,105,118]. The label-free aspect, automation and continuous monitoring of endothelial barrier function are the most significant advantages afforded by electrical techniques in comparison to macromolecular solute permeability studies.

Since the permeability of the plasma membrane towards ions is in most cases significantly lower compared to paracellular pathways (except for cases where paracellular permeability reaches the order of magnitude of electrical conductivity of the plasma membrane ion channels, e.g. endothelia of the BBB [114]), ion movement across a cell layer essentially describes the paracellular pathway and largely excludes transcellular solute transport mediated by vesicles.

As electrical techniques exploit Ohm's law, either a current or a voltage is applied across the cell layer. By measuring the respective returning voltage or current, the transendothelial electrical resistance (often referred to as TEER, or sometimes TER for *Trans-Endothelial/Epithelial Electrical Resistance*) is determined.

Filter-based electrical assays—Filter-based electrical setups (Fig. 2b) either apply a direct current (DC) and measure Ohmic resistance or inject a sinusoidal alternating current (AC) and measure the complex impedance of the system [12,114] (For a more detailed physical background on complex impedance we refer to excellent literature on impedance spectroscopy [8,62]). Since there is a constant concern that sustained exposure of cells to electric DC fields interferes with cellular processes due to membrane polarization or intracellular charge displacements [75], less invasive AC measurements are typically preferred for long-term monitoring of cell behavior. Nonetheless, DC measurements can be adequately used for experiments with short exposure times and those that do not require continuous monitoring. Many DC techniques use handheld chopstick electrodes and thus

still suffer from low parallelization and lack of automation. Since the filter itself significantly contributes to the overall resistance which cannot be separated from the cell layer resistance in DC measurements, the resistance of cell-free filters has to be measured in advance and subsequently subtracted.

In contrast to the rather limited information content of DC measurements, impedance spectroscopy that uses AC signals with discretely modulated frequencies within a spectrum mostly between 1 Hz and 10^6 Hz enables a more diversified study of the passive electric properties of the cell layer. Impedance, describing the electrical resistance in response to an AC signal, takes into account that capacitors become more conductive with increasing AC frequency. In a cell layer it is the plasma membranes that show capacitive behavior, storing charges at either side of their hydrophobic core. Thus, in addition to obtaining information on the resistance of barrier forming cell-cell junctions, changes in the cell layer capacitance are also detected. Changes in capacitance are an indicator for cell layer integrity or for example epithelial differentiation which is characterized by formation of microvilli [111]. Data collection at different AC frequencies also provides a reliable internal control for the setup whereby the resistance of the bathing fluid and contribution of the electrodes can be determined from impedance data without the need for control measurements on cell-free filters to be performed in advance. One of the first fully automated and computer controlled setup to perform time-resolved impedance based techniques for TEER measurements for a set of 12 filters has been described by Wegener et al. in 2004 [111] and is commercialized by Nanoanalytics GmbH (cellZscope).

TEER measurements using cells grown on porous filters, by either DC or AC techniques, are successfully applied for endothelia and epithelia that form very tight barriers, especially endothelia of the BBB [76,106,78,22], and renal and colon epithelial cells [82,45]. TEER values are typically normalized to a defined area of 1 cm^2, to allow for comparisons between barrier function measurements performed with different filter sizes. TEER values vary widely between endothelial cells depending on the vascular bed of origin. These variations are often a reflection of the cells' physiological function in the respective tissue or vascular bed. Human umbilical vein endothelial cells (HUVEC) for example show TEER values of about only 10 – 12 Ωcm^2 [29,88] while endothelial cells from brain capillaries that form the highly selective BBB exhibit TEER values of 250 – 500 Ωcm^2 when cultured *in vitro* [20,26,107] and even up to 1000 – 2000 Ωcm^2 in co-culture systems or when stimulated with hydrocortisone [20,107,43]. For relatively leaky endothelial cell layers with resistances of less than 5 Ωcm^2, as is the case for endothelial cells from the macrovasculature, filter based TEER measurements reach their detection limit and become incapable of resolving the impact of experimental manipulation on barrier properties with sufficient sensitivity. Even though impedance spectroscopy enables separation of cell layer resistance (R_{cl} = TEER) and cell layer capacitance (C_{cl}), it is not possible to separate contributions from the resistance of the cell-filter adhesion zone (R_{ad}) and the resistance from cell-cell junctions (R_j) [111,114]. This is especially problematic for rather leaky endothelia with less pronounced cell-cell junctions [58,114]. In a similar manner to macromolecular permeability, filter-based resistance measurements can suffer from leaks in the filter or defects within sites of the cell layer that can easily make readouts less reliable when these

defects remain undetected. Unfortunately, microscopic quality control of the cell layers can be difficult when filter supports are only semi-transparent and microstructured. Another critical aspect is the positioning of the electrodes, since heterogeneity and variability in electric fields (Fig. 2b, upper panel) can result in inconsistencies of TEER values. Changes in electrode positioning are especially likely to occur during experimental manipulation such as manual addition of agonists. Therefore, quantitative changes in TEER might not be exclusively due to stimulation of biochemichal pathways by the agonist. These inherent difficulties and the marginal improvements achieved with filter-based measurements created the driving force for developing alternative and more sensitive approaches.

However, certain aspects of filter based measurements should not be underrated. Filter based measurements have the great advantage that cell layers are accessible through the two compartments they separate. This allows co-culturing of endothelia or epithelia with e.g. fibroblast, pericytes or smooth muscle cells that can modulate differentiation and barrier properties [17]. Using permeable substrates, electrical studies can be combined with molecular permeability measurements as described above, so that a multi-parametric analysis can be performed on the same cell-layer. Recognizing these advantages, companies which initially have been focusing on solid substrate-based impedance techniques are recently developing filter-based alternatives.

Solid-substrate based electrical assays such as ECIS—The development of solid substrate-based techniques such as ECIS appeared to be a valuable alternative to filter-based electrical measurements. Filter based assays are important to the study of endothelial cells as cells grown on porous substrates are likely closer to their *in vivo* situation than cell growing on solid substrates. However beyond the technical difficulties that are discussed above, most of the other cell culture techniques such as microscopy, protein isolation and quantification, nucleic acid analysis, gene expression profiling, etc. are done with cells harvested from solid substrates. To properly correlate those results with barrier function properties, barrier function needs to be measured across cells grown on solid substrates. For this reason this paper focuses on the issue of preforming reliable and reproducible assays with solid substrate-based impedance methods.

In this case, cells are directly grown onto the electrode surface and thereby alter the impedance at the electrode-solution interface (Fig. 2d). Thin gold-film is the most commonly used electrode material since it is easy to pattern, has low specific resistance, is chemically inert, and highly compatible with surface modifications under physiological conditions (e.g. adsorption of zwitterionic cysteine followed by extracellular matrix protein adsorption). They are semi-transparent when used in thin layers of only 50 – 100 nm, allowing phase contrast microscopy. Indium Tin Oxide (ITO) is a transparent alternative to gold and is also compatible with florescence microscopy. Thin-film technologies allow miniaturization of electrode patterns down to the size of a single cell. This enables integration of impedance measurements to multi-well plate formats as used in high throughput screening. As an alternative to averaging values from a large cell population grown on one large electrode, multiple small electrodes can be positioned beneath the cell layer to create multiple individual measuring spots. Coplanar patterning of thin-film electrodes on cell culture ware makes solid substrate-based impedance measurements

consistent and compatible with *in vitro* cell culture, immunofluorescence staining and biochemical assays. Even combinations with other electrical methods that use thin-film electrodes can be easily achieved, such as *in situ* electroporation of cells [95], Quartz Crystal Microbalance (QCM) [44], Surface Plasmon Resonance (SPR) [68], that allow for multiparametric analysis of the cell culture. Substrate-integrated electrodes can either be arranged as interdigitated comb structures (IDEs) [31,71,92,5] or use a small working electrode (WE) in combination with a large counter electrode (CE) (Fig. 2d, middle panel), as is the case for ECIS (described in more detail below) and other non-commercialized setups [119,77,80,55,38]. Both strategies are aimed at making the impedance of the electrode-solution interface dominate over contributions from the bulk resistance, thus enhancing the sensitivity of the measurements to detect subtle changes in electrode coverage with cells or morphological changes within the cell layer. The WE/CE and IDE concept differ in the percentage of well coverage and relative contribution of opposing electrodes to the overall impedance signal. In the classical WE/CE approach with an area ratio of at least 1/100 suggested by Giaever and Keese the signal is dominated by impedance changes at the much smaller working electrode. In contrast, using interdigitated electrode structures changes at both electrode branches contribute to the overall measurement. IDEs can cover up to 80% of the well area, which means that the signal is averaged over a significant proportion of the cell population in a well, decreasing well-to-well differences and increasing dynamic range. With the WE/CE, only a small but defined population is probed, which can have the advantage that the population measured can be monitored in parallel by other means such as phase contract microscopy. The constriction resistance of the small WE creates a high sensitivity for minute morphological changes within the cell layer, which can be measured as cell metabolism-dependent impedance fluctuations also referred to as micromotion [39,56,57]. However, the requirement of a significantly larger counter electrode limits the abilities for miniaturization of the WE/CE concept.

ECIS and other substrate-integrated electric measurements allow for sensitive readouts on cell layer impedance even for non-barrier forming cells, such as fibroblasts [38] and highly invasive cancer cells [46,52]. In contrast to filter based methods, ECIS can thus be used for any adherent cell type to characterize cell behavior associated with changes in cell coverage or cell shape and cell layer architecture. ECIS applications range from measurement of cell attachment, spreading [113] and proliferation [121], to analysis of cellular micromotility [56,57,60] and lateral migration (i.e. wound healing assays) [47,85] to cytotoxicity studies [42,100,120] and monitoring of cell differentiation [7,87], and of course endothelial and epithelial barrier function [25,40].

ECIS is especially well-suited for the analysis of endothelial and epithelial barrier function, since individual impedance contributions from the intercellular cleft, the cell-electrode junction and the cell membranes can be distinguished according to a mathematical model developed by Giaever and Keese in 1991 [39]. Using this model, cell morphology and behavior within confluent cell layers can be defined by three model parameters R_b, α, and C_m which represent impedance contributions from the cell-cell junctions, cell-substrate junctions and membrane capacitance respectively [39,112] (described in more detail below

under *ECIS Setup and Principle*). Thus, contributions that specifically arise form barrier forming intercellular junctions can be distinguished [83,112,10].

3. ECIS setup and principle

ECIS setup

The ECIS technique is based on a coplanar thin-film gold two-electrode layout which is patterned on the bottom of a polycarbonate (Lexan™ or PET) cell culture substrate, as schematically depicted in Figure 3 (Fig. 3a - c) and described in detail in the figure legend. Adherent cells are directly grown onto the surface of the gold-film electrodes and the insulating polymer that confines the active electrode area to a defined geometry (Fig. 3a, b). The classical electrode design consists of one small circular working electrode (Ø ~ 250 m, $5 \times 10^{-5} cm^2$) and a counter electrode that is about 500 times larger (Fig. 3a, c). The 8-well arrays of this one electrode/well type are referred to as 8W1E. Other commonly used array types vary with respect to electrode size and layout as will be described below or are arranged in a 96-well format.

A schematic illustration of the electrical circuitry of the ECIS system is shown in Figure 3c. It includes the cell culture medium or any other physiological buffer as an ionic conductor between the two coplanar electrodes. In the classical 8W1E electrode layout, the small working electrode creates a bottleneck for current flow. Thus, changes occurring at the small working electrode dominate the measurement, while the contribution of the counter electrode becomes negligible. Cells adhering to the electrode, due to the insulating properties of their membranes, limit free current flow at the electrode-solution interface. Thus, the measurement becomes extremely sensitive to minute structural changes within the cell layer on the working electrode.

Measurement principle

Electrodes are probed with a weak non-invasive AC signal within a range of frequencies between 10 and 10^5 Hz and the frequency-dependent impedance (Z), which describes the electrical resistance in an AC circuit, is measured. According to Ohm's law impedance Z is defined by the ratio of voltage $V(t)$ and current $I(t)$. However, calculation of Z becomes challenging when phase shifts, as typically induced by capacitors or coils, between amplitude and current occur. Therefore, Z is viewed as a complex quantity, which can be graphically presented by a vector in a two-dimensional plane (Fig. 3e). The magnitude $|Z|$ denotes the length of the impedance vector and the phase shift ϕ describes the angle between the vector and the x-axis. Accordingly, complex impedance is often expressed as exponential function ($Z = |Z| \cdot e^{i\varphi}$). Alternatively impedance is defined by its Cartesian coordinates ($Z = Z' + iZ''$) that separate impedance contributions arising from current in-phase with the voltage (Z') from impedance contributions arising from 90° or out-of-phase currents (Z'') (Fig. 3e). In-phase impedance contributions (Z', along the “Real” axis) are termed resistance. Out-of-phase impedance contributions (Z'', along the “Imaginary” axis) are termed reactance and can include impedances arising from capacitive (Z_C) and, if applicable, inductive elements (Z_L). The prescript i is defined as $\sqrt{-1}$ and can be viewed as

a way to expand one-dimensional entities into two-dimensional ones, which is necessary to describe vectors such as impedance.

Figure 3d depicts how the ECIS system depends on the frequency of the injected AC signal, which is often illustrated by a so-called Bode diagram, plotting the impedance magnitude |Z| as a function of frequency (*f*) on double logarithmic scales. The graph shows respective typical impedance spectra for a cell-free system (grey line) and a system that includes a confluent cell layer grown onto the small electrode (black trace with filled circles).

The cell-free working electrode submerged in cell culture medium can be approximately described as a capacitor in series with an ohmic resistor (see Fig. 4a – c). The ionic bulk solution itself and the bottleneck effect of the small working electrode (Fig. 4b) define the ohmic resistance of the system (ohmic resistance arising from electrical wiring is small in comparison). Frequency-dependent polarization of the electrode surface submerged in ionic solutions leads to temporary accumulation of ionic species at the electrode-electrolyte interface (Fig. 4c). Consequently, a so-called electrical double layer forms, which approximately displays electrical behavior of a capacitor-like element (more accurately described by a Constant Phase Element (CPE) [64], an empirically derived electrical circuit element for non-ideal capacitive behavior). The Bode diagram for an 8W1E type cell-free electrode submerged in cell culture medium is shown in Figure 3d (grey line). For low frequencies the electrode capacitance dominates the |Z| spectrum as indicated by the declining slope of approximately – 1 (non-ideal capacitor). In the high frequency end, impedance becomes frequency-independent as the ohmic resistance of the bulk phase dominates.

When adherent cells are grown onto the electrode surface, they alter the impedance at the electrode-solution interface in a frequency dependent manner (Fig. 3d, black trace with filled circles). The impedance of the cell-covered electrode is increased compared to a cell-free electrode by Z_{cl} (Fig. 4d) within a certain frequency range (~ 100 Hz – 100 000 Hz for most cell types on 8W1E). The nature of the impedance contributed by the cell layer depends on the frequency of the probing signal. For relatively low current frequencies (100 Hz – 10 000 Hz), the current is forced to flow around the cell bodies, squeezing through the narrow clefts beneath and between neighboring cells (Fig 3d, section I delineated by red dashed lines; also see Fig. 4d, e blue arrows). This pathway is largely resistive in nature, and measurements in this frequency range (typically around 4 000 Hz) essentially focus on changes that occur in the cell-cell contact and cell-substrate contact regions of the cell layer. In endothelial barrier studies, this behavior at low frequency currents is used to probe for functional characteristics and stability of cell-cell junctions, namely adherens and tight junctions that critically control the passage of solutes, cells and fluid across the cell layer. At higher frequencies (> 10 000 Hz), the current considerably couples capacitatively across the cell membranes (Fig. 4d, green arrows) and lowers the cell layer impedance at the high frequency end of the spectrum (Fig 3d, section II delineated by red dashed lines). Monitoring cell behavior at high frequencies is therefore useful to assess processes that are associated with the degree of electrode coverage with cells. These cell-coverage dependent processes can be attachment and spreading after seeding of the cell suspension, proliferation, migration or cell death[113]. At intermediate frequency values, the current can represent a

mixture of both routes with varying contributions, resulting in a complex network of possible pathways (Fig. 4e, red arrows).

Modeling of ECIS Data

Comparison of an experimental setup to a network of ideal electric circuit elements such as Ohmic resistors and capacitors is a common practice in impedance spectroscopy and equivalent circuits are usually developed that show similar electric frequency response to the experimental system. The total impedance of this equivalent circuit is calculated using Ohm's and Kirchhoff's laws depending on the respective arrangement of individual model elements (e.g. Fig. 4). This allows deriving a mathematical transfer function; fitting the transfer function to the experimental data finally provides estimates for the individual impedance contributions of the system. This approach is routinely applied for filter-based impedance measurements. The following parameters can be extracted from filter-based-measurements as described above in “filter-based electrical assays”: R_{bulk} for the resistance of the medium, filter and wiring; C_{el} for electrode capacitance; R_{cl} for the ohmic resistance of the cell layer (mostly defined as TEER [Ωcm^2]); and the cell layer capacitance C_{cl}.

To analyze impedance spectra obtained with ECIS Giaever and Keese developed a transfer function by using a slightly modified approach that is based on the derivation of differential equations and corresponding boundary conditions [39]. Three model parameters that describe properties of the cell layer can be extracted from the transfer function: α, R_b and C_m (Fig. 5a). The parameter α is a measure for the constraint of current flow within the subcellular cleft. The value of α depends on the cell radius r_c, the average distance d between electrode surface and the cell bodies as well as the specific resistivity ρ of the electrolyte in the subcellular space ($\alpha = r_c(\rho/d)^{1/2}$). The parameter R_b is a measure for the electrical resistance in the intercellular clefts and is highly influenced by the tightness of cell-cell contacts. Changes in the cell radius can also affect R_b since a reduction of the total sum of intercellular spaces increases the resistance across the cell layer. Membrane properties are represented by the model parameter C_m. C_m is influenced by membrane composition and morphology such as the formation of microvilli in the apical side as is the case for many epithelial cells. Figure 5b illustrates the respective influence of changes in α, R_b and C_m on frequency-dependent course of |Z|. By fitting the transfer function to the experimental data of confluent cell layers on ECIS electrodes (Fig. 5c; shown only for HDMEC for clarity), cell-type specific values for α, R_b and C_m can be extracted. The table in figure 5d shows the results from α, R_b and C_m analysis on HDMEC, HUVEC and, as a non-endothelial example, rat vascular smooth muscle cell (RVSMC) layers. The difference in barrier function of these three cell types is especially reflected by their respective R_b values. Thus, α, R_b and C_m analysis of impedance spectra can be extremely useful to assess endothelial cell layer quality.

4. Experimental settings and practical guidelines

Monitoring parameters

As described above, recording of an impedance spectrum provides information on the frequency-dependent behavior of the entire system under study, not only the cell layer

(described by Z_{cl}), but also the electrode capacitance and bulk resistance including electrical wiring. During ECIS data acquisition, for each selected frequency both the impedance magnitude |Z| and phase shift ϕ between current and voltage are recorded, from which the resistance (real part of the impedance *Z*' or the in-phase impedance) and reactance (imaginary part of impedance *Z*", or the 90° out of phase impedance) can be calculated. Whereas |Z| contains information on both resistive and capacitive behavior of the system, resistance reflects only the resistive contribution and reactance reflects only the capacitive contribution. In this system, $Z' = R$ and $Z'' = 1/2\pi fC$ and thus $C = 1/2\pi f Z''$. Note that due to frequency-dependent impedance contributions of resistance and reactance, the magnitude of these quantities is also frequency-dependent. This means that if data are presented as a function of resistance (*R*) it only reflects the portion of system impedance that behaves as an Ohmic resistor. Cell layer contributions to resistance arise at the intercellular and subcellular clefts. On the other hand, capacitance (*C*) data mirrors the reactance of the system and neglects the resistive contribution. Cells change the capacitance of the system due to the capacitive behavior of their plasma membranes. Consequently, the choice of which parameter to monitor, impedance magnitude, resistance or capacitance depends on the focus of the study. Capacitance readings at high frequencies (e.g. 40 000 Hz, see spectrum in Fig. 3d, section II) are useful in documenting changes in electrode coverage, such as attachment and spreading, proliferation and migration. *R* and |Z| between 400 Hz and 4000 Hz (see spectrum in Fig. 3d, section I) are typically chosen to assess changes within paracellular pathways, such as changes in cell morphology and barrier function.

To illustrate the differences between these monitoring parameters figure 6a shows attachment, spreading and differentiation of an HDMEC cell layer followed over time by means of impedance magnitude (|Z|, black curve) resistance (*R*, red curve) and capacitance (*C*, blue curve). The time course of capacitance at 40 kHz, which is sensitive for the degree of electrode coverage with cells, indicates that a confluent cell layer is established after 48 h (Fig. 6a, blue curve). In contrast, HDMEC cell layer resistance (*R*) at 4 kHz, the parameter for barrier function, continuously increases over the entire 90 h of data acquisition, until a maximum resistance of about 3 500 is obtained (Fig. 6a, red curve). In compliance with the electrical data fluorescent staining of VE-cadherin and the actin cytoskeleton in HDMEC cell layers at different time points after seeding (Fig. 6b) revealed ongoing cytoskeletal re-arrangements and increased colocalization of actin and VE-cadherin after 96h as compared to only 24h. |Z| at 4 kHz shows a similar behavior to *R*, but with slightly higher magnitude (Fig. 6a, black curve).

Frequency spectra for |Z| and *R* for cell-free-and HDMEC cell-covered 8W1E type electrodes are shown in Figure 6c, f and those of the ratios of cell-covered/cell-free for |Z| and *R* are depicted in Figure 6d, g. The maxima of these ratios indicate the respective frequencies with the broadest range of relative change in |Z| or *R* (Fig. 6d, g) and these represent the optimal frequencies that should typically be used in sensitive ECIS measurements. The higher the number of different frequencies applied to the system, the lower is the temporal resolution of the measurments. For instance, in cases where the cell layer responses are fast and only transient (e.g GPCR stimulation with histamine), the speed of data acquisition can be critical and as such instead of successively recording whole

frequency spectra, the number of measurement frequencies should be limited to only one or few selected frequencies. In the example shown in figure 6e a whole spectrum was initially recorded to determine the optimal frequency (in this case 2 kHz) with the maximum dynamic range of $R_{cell\text{-}covered}/R_{cell\text{-}free}$. Then, the response of the cell layer to histamine stimulation was monitored at this selective frequency as a function of time (Fig. 6e, h). For studies on endothelial barrier function, *R* is often preferred over |Z|, since resistance readings exclusively mirror the purely resistive contributions. *R* is thus reflective of changes that occur at cell-cell and cell-substrate junctions. Figure 6e and 6h show the respective time course of |Z| and *R* of the same measurement. While Δ|Z| and Δ*R* after HDMEC barrier disruption by histamine represent approximately 2000 Ω, normalizing this value to the initial baseline values translates into a 6.6% change in |Z| but an 8.3% change in *R*.

Resistance versus TEER and R_b

TEER is a well-established term that originates from transfilter measurements and is also frequently used to describe data obtained with solid substrate-based electrical measurements. We want to make the reader aware of the differences in TEER between data obtained from filter-based and solid-substrate based impedance measurements. TEER classically describes the resistance of the cell layer only (see chapter: "*overview of endothelial barrier function assays*"). Routinely, in filter-based measurements TEER is obtained by either subtraction of the resistance of the empty filter and bulk solution or by equivalent circuit calculations. TEER values are conventionally normalized to a surface area of 1 cm^2 to give specific TEER values in Ωcm^2. One should keep in mind that TEER cannot distinguish between contributions from cell-cell junctions and resistance arising in the subcellular cleft. In contrast, the resistance values typically plotted for ECIS measurements do not include routine subtractions or adjustments for electrode size. Moreover, ECIS resistance readout includes in-phase impedance contributions of the entire system, arising from the cell layer itself, the electrode-electrolyte interface, bulk resistance and wiring. The most accurate way to extract a TEER equivalent value from ECIS data is *via* the mathematical model that separates the parameters R_b, α and C_m. R_b describes the resistance arising from the cell-cell junctions and is reported as Ωcm^2, a with units of $\Omega^{1/2}cm$ is the the impedance contribution from the subcellular cleft, and C_m describes the membrane capacitance reported in $\mu F/cm^2$. R_b is closest to a TEER value measured by other means (CellZScope, Chopsticks) but is substantially less in magnitude since the resistance from the subcellular cleft is substracted. Time-dependent ECIS model analysis on consecutive impedance spectra can be used to study the effect of agonists on individual changes in cell-cell, cell-substrate contacts or changes in membrane capacitance, respectively [83,72]. However, the legitimate rationale why most ECIS users plot resistance instead of R_b time courses is to enhance the temporal resolution of the measurements. Indeed, in order to extract R_b, a whole frequency spectrum needs to be recorded for each time point. When data is measured at a single frequency, the temporal resolution of the measurements is about 20 times higher (0.5 seconds per well at one frequency versus 10 seconds per well at 11 frequencies). One should keep in mind that R_b is a model parameter derieved by applying a mathematical model to the data from biological samples. The model is based on certain assumptions: (i) the electrode is covered with a confluent cell layer (ii) the cells are regarded as circular discs with a uniform average radius r, in uniform average distance d above the electrode (iii) the current flows radially in

the space between the basal membrane and the electrode surface (iv) the current density does not change in z-direction [39]. These assumptions might not always hold true for the experimental situation and the implications of deviations from these assumptions are not completely understood. Thus, changes in R_b should be critically evaluated, when the situation on the electrode is suspected to be significantly different from the model assumptions. The most accurate calculation of model values are expected when the cell layer is confluent, without defects, and homogeneous with respect to cell size. The cell structural architecture, such as components of the cytoskeleton, cell-cell and cell-substrate junctional complexes, can be assessed by immuno-histochemical staining of the cell layers on the electrodes after an ECIS experiment. This allows changes in cell-cell junctions reflected by R_b to be validated using diverse microscopic techniques or molecular permeability assays. However the validity of the ECIS parameter α is much more difficult to assess by alternative methods and may explain the *hitherto* limited use of α quantification in endothelial barrier function analysis. However, a recent study showed that changes in α correlated nicely with changes in adherens junction regulation[2].

Monitoring frequency

Endothelial barrier function measurements are typically recorded using the in-phase Impedance (Resistance) at 4 000 Hz. This frequency was used by Giaever and Keese in their first paper on the subject [38] and set precedent for using 4000 Hz in ECIS measurements. The selection of this frequency was purely happenstance (personal communication) and thus a scientifically critical look at frequency selection is warranted. As a general guideline, the sensitive frequency for detection of changes in cell layer properties can be determined by dividing the resistance of a cell-covered electrode by the resistance of a cell-free electrode. When these ratios are plotted for each individual frequency one obtains a curve from which the maximum ratio reflects the frequency with the broadest range of relative change in resistance (Fig. 6g, 7b). This optimal frequency is cell-type specific (Fig. 7a, b) and has to be determined empirically, but in most cases it ranges between 1000 and 6000 Hz. Fig. 7b shows that the optimal frequency for HDMEC is around 2000 Hz while that of HUVEC is around 4000 Hz and that of primary aortic rat vascular smooth muscle cells (RVSMC) is between 5000 and 6000 Hz. For cells that form very tight barriers such as endothelial cells from the BBB, the optimal monitoring frequency can be as low as 400 Hz. While this gives the frequency at which we have the greatest dynamic range between cell-free and cell covered electrode, it may not reflect the frequency at which we have the greatest dynamic range for a given assay. For example in figure 7c, the resistance drop upon HDMEC stimulation with histamine is more pronounced at 400 Hz as compared to 4000 Hz. This is in spite of the fact that at 4000 Hz $R_{cell\text{-}covered}/R_{cell\text{-}free}$ is maximal for this specific cell layer on 8W10E+ type electrodes (see comparison of different electrode types in the next paragraph) (Fig. 7c, inserted graph). This discrepancy between the maximum of $R_{cell\text{-}covered}/R_{cell\text{-}free}$ and the empirically higher sensitivity at 400 Hz arises from the fact that the extrema of our assay is not cell-free / cell covered, but cell covered and perturbed /cell covered. For barrier function assays the dynamic range of interest is limited to the state of cell-cell junction functionality in confluent cell layers (Fig. 7e). By plotting the difference in R before and after agonist addition as a function of frequency, it becomes obvious that the dynamic range of the response increases towards lower monitoring frequencies (Fig. 7f).

Thus the frequency for any assay can be optimized by calculating a frequency plot of ($R_{start} - R_{(max\ response)}$)/$R_{start}$ × 100 (Fig. 7g), referred to here as frequency response index (FRI), where R_{start} is the resistance of the fully maturated cell layer before manipulation and $R_{(max\ response)}$ is the absolute resistance at the maximum response after agonist addition. Ideally the FRI is determined using the maximum stimulation according to a dose-response experiment. For the histamine experiment a maximal change in resistance of 27 % is indeed obtained for a frequency of 400 Hz. This refined approach can be choosen when a maximal dynamic range and sensitivity is desired for a specific assay. However, endothelial barrier measurements at 4000 Hz are historically established and therefore choosing this frequency allows for better comparison with the abundant data from the current literature. While monitoring endothelial cell behavior at 4000 Hz is non-optimal, the decrease in resistance when tight junctions open remains consistent. Thus using 4000 Hz is as legitimate as using lower frequencies.

Using resistance to measure barrier function does have a potential artifact. Choosing too high frequencies for monitoring changes in barrier function causes increases in resistance after histamine addition (Fig. 7c, black trace). This effect, which can be disastrous for correct data interpretation, can be explained by taking a closer look at the resistance spectra obtained from HDMEC and HUVEC (Fig. 7a). At high frequencies (> 10 000 Hz) the resistance spectrum of HDMEC which are known to form tighter cell-cell junctions than HUVEC bends below the spectrum of HUVEC and below that of the non-barrier forming RVSMC. Thus, when the selected monitoring frequency is too high, the actual decrease in barrier integrity artefactually translates into an increase in barrier function. This behavior is also correctly reflected by the frequency response index (Fig. 7g) and can thus be avoided by FRI analysis. In contrast, when impedance is chosen as the sensitive monitoring parameter, instead of resistance, selecting a high frequency will affect the sensitivity of the signal but not its quality (Fig. 7d).

Electrode size and layout

The surface area of the effective electrode has to be considered when selecting optimal monitoring frequency (Fig. 8). The smaller the radius (r) of a circular electrode, the larger the constriction resistance (equaling $1/r$) and the greater the contribution of impedance from the electrode-solution interface (equaling $1/r^2$; with or without cells) to the overall impedance. This electrical behavior explains how variations in the electrode size and electrode layout can alter contributions to the overall signal and lead to changes in sensitivity. In general, a smaller electrode area, creates a higher sensitivity towards changes at the electrode-solution interface and therefore at the electrode-cell layer interface. However, the size of the cell population from which the measurement is made shrinks with decreasing electrode size, providing less statistical coverage of the cells studied. Furthermore, with very small electrodes, parasitic impedance contributions arising from stray capacitance within cables and measuring equipment become problematic. Therefore, electrode sizes below $5 \times 10^{-5} cm^2$ (e.g. the 8W1E described so far, Fig. 8a) are rarely used.

Figure 8a, b and c illustrate the three different electrode types frequently used in the study of endothelial barrier function 8W1E, 8W10E and 8W10E+ respectively. The first electrode

layout of ECIS, the 8W1E arrays comprise one circular working electrode with a diameter of 5×10^{-5}cm^2 which has been created by photolithographic techniques as an opening in the insulating polymer, and about 500 times larger counter electrode in each well (Fig. 8a). A caveat of the classical 8W1E electrode type is that measurements represent only a small fraction of the cell layer, which, depending on the cell type, typically ranges between 20 – 100 cells (see for example Fig. 3b with ~ 30 HDMEC cells on an 8W1E electrode). Especially in cases where the cell monolayer is heterogeneous, a small sampling area can become problematic, as one may encounter high well-to well variability. The 8W10E type electrodes have ten electrode openings of 5×10^{-5}cm^2 each (Fig. 8b), which provides an active surface area ten times larger compared to the 8W1E electrodes. Measurements with the 8W10E type electrodes thus increase statistical coverage across a larger cell population and exhibit lower total resistance compared to 8W1E electrodes (Fig. 8d), but only slightly decreases the sensitivity (Fig. 8e). The ability to average data from a larger cell population can be advantageous when basal constitutive fluctuations in cell shape within the monolayer must be distinguished from large responses to experimental manipulation, such as agonist stimulations, pharmacological or molecular manipulations (Fig. 8g, h). The 8W10E+ layout offers an even better statistical coverage of the cell layer than the 8W10E arrays. In this setup, a total of 40 electrode openings are evenly distributed over the 0.8cm^2 well surfaces (Fig. 8c). To achieve this, the 40 electrodes are lithographically patterned on an interdigitated finger structure, by creating 20 gold openings for each electrode and counter electrode. Despite the entirely different layout of 8W10E+ electrodes, they retained the “10E“ nomenclature due to the similar electrical behavior they share with the 8W10E electrodes (see spectra in Fig. 8d). One notable difference is that while 8W1E and 8W10E electrodes distinguish between a small working electrode and an at least 100 times larger counter electrode, this is not the case for the 8W10E+ where all 40 gold surfaces contribute equally to the overall measurement. An important caveat to keep in mind is that with any given cell type plated on any given electrode, the optimal frequency has to be determined empirically (Fig. 8e) as this frequency can change depending on the quality of the cell layer in terms of species of origin, vascular bed, cell passage number, cell isolation and culture conditions. Figure 8f shows a wide variability of the optimal frequencies (ranging from 1414 to 8000 Hz) obtained from 49 (on 8W1E) and 61 (on 8W10E+) independent cell populations of HDMEC originating from different cell isolations (different donors) and different passage numbers. The difference in electrode size (e.g. 8W1E versus 8W10E+) leads to an overall shift in the optimal frequencies (Fig. 8f).

Normalization of raw data

A historically rooted practice is the presentation of data as normalized values (Fig. 9). In this case, resistance or impedance magnitude at each time point are normalized to baseline values either at time zero or before manipulation of the cell layer, such as addition of an agonist. However, normalization can hide flaws in the raw values, especially when cell layers with different baseline values are compared (Fig. 9a). A difference in basal cell layer resistance typically reflects an inherent difference in barrier function and thus cell layer integrity, maturity, and architecture. Therefore, the effect of an experimental manipulation, such as the addition of an agonist (in this case the inflammatory agonist thrombin) inevitably results in responses of smaller size and slower kinetics in the condition with lower baseline

resistance (Fig. 9b). In the example given in figure 9a, b cell layers of different maturity were used. When HDMEC cell layers that have been cultured on the electrode arrays for 48h, 72h or 96h (seeded at a cell-density of 100 000 cells/cm^2) were subjected to thrombin stimulation, both the baseline resistance of the cell layer and the magnitude of resistance drop after thrombin stimulation increased with time in culture (Fig. 9a). Normalization of these data hides the differences in baseline resistance and leads to respective over- or underestimation of the impedance drop (Fig. 9b). As compared to figure 6a, HDMEC need about 3 - 4 days to establish a fully matured cell layer with maximum electrical resistance. Consequently, the dynamic range between fully established barrier and by thrombin disrupted barrier is maximal for the fully matured cell layer. A quantification of the relationship between baseline resistance and the magnitude of resistance drop after thrombin addition (Fig. 9c) clearly revealed that the intensity of response is dependent on initial cell layer resistance. When barrier disrupting effects are to be monitored, cells have to be cultured on the arrays for at least 72 h, when cell layers have reached basal resistances of about 3000 Ω or more (Fig. 6a, Fig. 9a).

Cell culture

Every cell type will have a specific optimal layer resistance that should be determined empirically and will behave differently depending on species of origin, vascular bed, passage number, seeding densities, array-surface preparation and cell culture on the ECIS array.

The time of cell culture on the array critically influences maturation of cell-cell junctions and response to agonist stimulation as illustrated in figure 9a. Moreover, influences from cell passage number, isolation procedure and source can significantly affect the basal resistance of cultured endothelial cells (Fig. 9d, e). HDMEC cell layers of low passage number (P6) can reach a resistance of over 4000 Ω, whereas high passage number HDMEC (P12) cell layers tend to be limited in their barrier forming capabilities reaching only resistances of 2500 Ω or less, as has been observed for other cell batches with passage numbers above P9 (Fig. 9d). As repeatedly mentioned low basal cell layer resistance limits the dynamic range of agonist response (Fig. 9e). Other cell culture parameters can influence the quality of the cell layer, which can include pre-coating of the electrodes with extracellular matrix (ECM) proteins, time of serum starvation before agonist addition or differences in medium composition, especially regarding content of growth factors such as VEGF. For example, when culturing of HDMEC cells on ECIS arrays, several aspects have to be considered. Since cells do not bind directly to the electrode surface, but rely on molecular interaction of their integrins to extracellular matrix proteins that contain the RDGS binding sequence, cell attachment and spreading depends on pre-absoption of proteins to the electrode surface. In all presented examples ECIS electrodes were prepared by pre-absorption of denatured collagen (gelatin, 0.2 % in PBS) to promote integrin-dependent cell-attachment and spreading. Alternatively to this low cost coating substrate, defined extracellular matrix (ECM) proteins such as collagen IV, fibronectin, vitronectin or laminin can be used in either pure form or in mixture. Different ECM proteins are attributed with distinct roles in vascular morphogenesis, stabilization, endothelial proliferation and survival [24] and thus, depending on the biological question, the choice of protein for

electrode coating can become important [6,54]. To our knowledge it has not been established, to what extent different protein coatings of *in vitro* substrates modulate histamine, thrombin or S1P signaling in mature endothelia. Through the activity of proteases and de-novo synthesis of ECM proteins endothelial cells constantly modify the composition of their basement membrane. Differences in medium composition can significantly influence endothelial cell maturation. The medium supplement hydrocortisone helps HDMEC cell layers in reaching higher and more stable resistances, while a lack of hydrocortisone, especially when ascorbic acid is included in medium, decreases baseline resistance and induces periodical oscillations (data not shown). Hydrocortisone and ascorbic acid seem to have positive effect on recovery of baseline resistance after stimulation with histamine or thrombin (data not shown). In fact, a barrier stabilizing effect on endothelial cells from the blood brain barrier has been shown for hydrocortisone and other glucocorticoids, as they increase adherens junction and tight junction protein expression and induce cytoskeletal re-arrangements [43,115]. A barrier stabilizing effect of ascorbic acid was linked to an increase in collagen synthesis, an extracellular matrix component of the endothelial basal membrane [104].

For some agonists, serum starvation helps in increasing the responsiveness of the endothelial cell layer to the respective agonist. Changes to low serum media (basal medium with 0.3 % serum) were found to enhance the basal resistance of HDMEC cell layers after between 6 – 24 h of serum starvation and positively influence the responsiveness to histamine and thrombin (data not shown).

An important factor to consider when working with primary endothelial cells which is the cell source; different batch of cells originating from different pools of small donor population will behave differently. HDMEC obtained from three different isolations seeded at low passage number (P5) at the same initial cell density show differences in cell layer maturation. Cell layer resistance 4 days after seeding differed significantly for the three isolations, as the values included in figure 9f indicate. Thrombin stimulation resulted in a typical response profile for all three isolations, although the kinetics of cell layer recovery to baseline resistance varied significantly (Fig. 9f). Although most often discrepancies in cell layer response to inflammatory agonists can be attributed to variability in basal endothelial cell layer resistance, it is highly likely that the cells' genetic and epigenetic programs are additional factors that influence the responsiveness and recovery potential of the endothelium.

For this and all other caveats discussed so far, it cannot be overstated that other endothelial cell types isolated from different species and/or different vascular beds might respond differently and the above discussed parameters have to be determined empirically for each endothelial cell type. Therefore, we recommend an initial full characterization of typical electrical behavior of each given cell type on ECIS electrodes under optimal culture conditions prior to the actual experiment. Ideally, the cell culture is monitored for a broad frequency range ($10 – 10^5$ Hz, at 11 – 20 distinct frequencies) starting from cell inoculation onto the ECIS electrodes until the decease of the culture, and including all necessary media changes. Data from such experiment will provide valuable information on (i) time until and value of maximum resistance/impedance for each selected frequency (ii) frequency with

maximum sensitivity for the given cell type and array type (iii) cell-type specific optimum time frame for a given assay. Moreover, such data set includes valuable reference data (i.e. typical baseline resistance/impedance) as a basis for quality control of cell layers in future experiments. In this light also α, R_b, C_m analysis of frequency spectra recorded at ideal experimental conditions can serve as additional look-up parameters for quality control and cell-type specific characterization. Unfortunately, the common practice of publishing ECIS data as normalized values hides a lot of valuable information on cell-type specific electrical properties.

Pharmacological and molecular manipulations

Studies aimed at determining the molecular players involved in the regulation of endothelial barrier function often use pharmacological or molecular manipulation of the cell layer. For manipulation of different signaling molecules and pathways cultured endothelia can be subjected to pre-incubation with various pharmacological inhibitors or activators before the receptor agonist is added. Targets of these pharmacological pretreatments typically are cytoskeletal proteins [14], kinases [51,59], GTPases [123], phospholipases [48], phosphodiesterases [51], ion channels [90] or second messengers such as calcium [65,16] or cAMP [93]. Because of limited selectivity of pharmacological drugs and consequently difficulties in accurate interpretation of results without ignoring possible off-target effects, manipulation of cells using molecular approaches are becoming more and more common. By ectopic expression of cDNA encoding either wild type or mutated/truncated protein variants, or protein knockdown using siRNA or shRNA the levels of specific proteins a can be elevated or decreased. By this means the effect of ectopic expression or knockdown are studied on either endothelial barrier maturation [1] or in response to agonist stimulation [11,110]. Strategies such as “erase and replace“ experiments combine both approaches, starting with an siRNA- or shRNA-mediated knockdown of the protein of interest and followed by expression of either a wild-type control or a mutated/truncated form of the same protein [41,90]. Unless stably transfected cell lines or isolates from knock-out animals are used these techniques require transfections or viral infections of cells prior to seeding on ECIS electrodes or during cell layer maturation on the array [110]. And thus, these manipulations evoke additional challenges in ECIS assay reproducibility, which can essentially be narrowed down to (i) transfection efficiency and (ii) survival rate. These parameters are of special concern in ECIS assays, as the electrodes beneath the cell layer can only probe a fraction of the cell layer and cannot be selected according to local transfection efficiency. In a cell layer with a transfection efficiency of 80% it is still possible that none of the cells on the actual electrode is actually transfected (extreme case, 8W1E). *In situ* electroporation using the ECIS electrodes to introduce siRNA, cDNA or other macromolecules into cells [95] could provide an interesting possible solution, as transfection is restricted to the cell population directly on the electrode. Toxic side effects of transfection reagents or massive protein overexpression can significantly affect survival rate and the process of cell layer maturation, and as a consequence baseline resistance of the cell layer. This is especially problematic when differently transfected populations are to be compared and reveal an offset in baseline resistance. Observed differences can be a result of the actual molecular manipulation or merely due to differences in survival rate and cell layer maturation timeline. Therefore, in all experiments that include pharmacological treatment or

molecular manipulation of the cell layer, it is important to pay attention to absolute resistance/impedance values of the cell layer.

Agonist addition and preparation

For monitoring of fast cell layer responses to GPCR stimulation the agonist has to be added during data acquisition which requires manual fluid handling in a common laboratory setting. The method of delivery of the agonist solution to the cell layer and the volume of that agonist solution is critical (**Fig. 10 a – d**). Addition of agonists in very low volumes (e.g. 2 μL of a 200 × stock to a final cell well volume of 400 μL) may delay cell responses due to the time required for diffusion of such small volume and thereby influence reproducibility, as we illustrate for addition of thrombin to HDMEC cell layers on 8W10E+ type electrodes (see **Fig. 10a, d**). On the other hand, addition of very high volumes (e.g. 200 μL of 2 × stock) introduces an artefactual contamination of the agonist response with the cells' reaction to physical stimuli such as shear stress and temperature changes (**Fig. 10c, d**). A mere opening of the incubator in order to add of the agonist solution to the wells transiently increases HDMEC cell layer resistance by about 100 Ω (data not shown). As a general guideline, addition of 20 μL of 20 × agonist solution (e.g. 100 nM of thrombin for a final concentration of 5 nM) yields maximal reproducibility and causes the least disturbances to the cell layer (**Fig. 10b, d**). The agonist in 20 μL is ideally added into the middle of the well, by dipping the pipet tip just below the fluid meniscus and steadily and slowly releasing the agonist solution into the fluid.

For some agonists a proper preparation of the agonist solution can be crucial for the success of the experiment. In ECIS experiments with HDMEC, for example, we found that the response profile to S1P addition significantly changed with different preparation of the agonist stock solution (**Fig. 10e**). When the S1P stock was prepared from a methanol containing solution, HDMEC showed a multi-phasic response with a first transient increase of resistance for up to 5 min followed by a decrease slightly below baseline values and a final more sustained increase (**Fig. 10e**, grey curve). By removal of methanol residues from S1P through evaporation under a dry nitrogen stream before re-suspension in low serum medium, increased HDMEC resistance in response to S1P was sustained (**Fig. 10e**, black curve). The magnitude of the HDMEC monolayer response to S1P could be further enhanced by adding a final concentration of 0.03 mg/ml fatty acid-free BSA to the agonist solution (**Fig. 10e**, red curve). S1P is poorly dissolvable in organic solvents and in aqueous solutions unless it is bound to an amphiphilic carrier [84]. In blood serum albumin is the major physiological carrier of lipids after HDL and LDL [73]. It has been shown that BSA is required for S1P solubilization after release from platelets [50] and that S1P bound to these natural lipid carriers is potent in activating S1P receptors on endothelial cells [117].

6. Concluding Comments

We have described the practical guidelines and challenges of basic endothelial barrier function ECIS assays using wild type endothelial cell layer stimulated with GPCR agonists such as thrombin, histamine and S1P. This protocol can be easily adapted to include additional treatments and manipulations of the endothelial cell layers. Of course, applications can be adapted to the study of other agonists that impact on endothelial barrier

function such as vascular endothelial growth factor (VEGF) [10,14], Bradykinin [83], tumor necrosis factor α (TNFα) [86,91], lipopolysacharides (LPS) [15,16,18] or Prostaglandin E2 (PGE2) [51]. However, the time of cell response might differ significantly. While thrombin and histamine as typical GPCR agonists evoke transient changes in barrier function, agonists like VEGF act over a time course of hours. Because of limited selectivity of pharmacological inhibitors and consequently difficulties in accurate interpretation of results without ignoring possible off-target effects, manipulation of cells using molecular approaches including introduction of cDNA, and siRNA become more and more common. In all experiments that include pharmacological treatment or molecular manipulation of the cell layer, it is important that the ensuing effects on basal cell layer resistance and on the response to agonist stimulation are not viewed independently. Differences in basal cell layer resistance between otherwise identical experimental conditions can affect the intensity and kinetics of response to agonist stimulation, pharmacological treatment and intracellular manipulations of molecular pathways. Therefore, experimental manipulation that resulted in cell populations with different baseline monolayer resistance values is likely to generate misleading results and such data should be interpreted cautiously. Because ECIS can provide information on the basic passive electrical properties of an endothelial cell layer and its barrier properties, ECIS can also be used to determine the quality of primary cell isolations [13].

Even though the current manuscript is tailored to endothelial research, similar considerations and guidelines apply to epithelial barrier studies. Common properties of endothelia and epithelia are the formation of selective barriers between two compartments, which are established by the formation of well-regulated cell-cell junctions, most importantly adherens junctions and tight junctions. However, the molecular organization and topology of endothelial junctional structures is more variable and less restricted as compared to epithelial junctions. In endothelia, adherens junctions, tight junctions and gap junctions are often intermingled to form a complex zonular network at overlapping strands of adjacent endothelial cells, while in epithelia different junctional complexes are generally found at distinct topologies along the intercellular cleft [108]. Differences in molecular composition of junctional proteins exist, as some of them, such as VE-cadherin and the TJ protein Claudin-5, are exclusively found in endothelia [108]. Even though cadherins crucially contribute to the formation and stability of cell-cell-junctions, barrier function can be majorly ascribed to the existance of tight junctions. Expression levels of tight junctional Occludin seem to correlate with the permeability of endothelia from different vascular beds, with highest expression levels reached in the BBB [9]. As opposed to most endothelia tight junctions of epithelia, due to their distinct role in selective transport and filtration, are often better developed and equipped with ion selective Claudins. Thus, the relative benefits of solid-substrate based electrical measurements versus conventional filter based tracer permeability may change depending on the biological question and type of endothelium or endothelium under study. Generally speaking, the same recommendations discussed herein for ECIS measurements using endothelial cells can be applied to epithelial cells. For any given cell type, we recommend an initial experiment recording the kinetics of attachment, spreading and cell layer maturation; this will provide the basis for establishing the cell

culture protocol on ECIS electrodes and for defining the suitable monitoring parameters such as frequency and temporal resolution.

It is worth mentioning that other aspects of ECIS such as wound healing assays, monitoring of cell proliferation and micromotion analysis can also be exploited to analyze endothelial and epithelial cell behavior in response to pharmacological and molecular manipulations, as recently summarized in an online video protocol [98]. In the wound healing assay, elevated electric fields are used to selectively induce a lesion that is restricted to the electrode area. Time dependent repopulation of the “electrically-wounded“ cell-free area is then recorded electrically to obtain information on the migratory behavior of endothelial cells [33]. Analysis of cell adhesion upon cell seeding on electrodes can be useful in identifying the molecular players involved in the regulation of cell-matrix interactions [81,101]. Similarily, micromotion analysis has been used to quantify small and fast rearrangements of the cell-cell junctions [97]. The introduction of 96-well assay format provides means for high-throughput screening and enhanced statistical analysis. Future platforms combining Impedance measurements with optical measurements will offer means to simultaneously determine Impedance and protein localization and movement or measure ions and second messengers in real-time; these tools will provide powerful means to study the molecular signaling mechanisms associated with cell functions.

Finally, as far as scientific interpretations of biological responses and their extrapolations to the physiological situations are concerned, caution should be applied as ECIS is an *in vitro* technique that studies cells in culture outside of their *in vivo* context. Endothelial as well as epithelial cells in culture do not fully recapitulate the *in vivo* situation and any extrapolation of ECIS data to the *in vivo* condition has to be backed by additional methods such as *in vitro* co-culture systems or ideally *in vivo* measurements of permeability from isolated intact tissues or whole animals. One of the major discrepancies between the *in vitro* assay and *in vivo* situation is that ECIS is based on a rigid cell-electrode surface and does not allow for accumulation of a measurable substrate (e.g. albumin) into either the luminal or abluminal side. Thus, changes in endothelial and epithelial cell layer resistance measured with ECIS cannot reflect any tension or volume adjustments that would normally occur in soft tissues. ECIS measurements on a rigid substrate might thus lead to an under – or overestimation of endothelial barrier disruption upon exposure to inflammatory agonists. An underestimation of the severity in endothelial barrier breakdown can be anticipated, when regarding the fact that the ECIS *in vitro* system cannot account for effect of hydrostatic pressure that might aggravate cell-cell disruption in an *in vivo* setting. However, it has also been shown that mechanical forces on intact endothelial cell layers can enhance barrier properties [79,27,103] and thus might render the endothelium less sensitive to agonist-induced barrier disruption in the first place. Another view is that the rigid substrate cannot adapt to tensile forces as it is possible in the much more flexible basal membrane of the blood vessel. Such flexibility of underlying tissue might allow for considerable compensations to encounter endothelial contractile forces that lead to the often observed dramatic intercellular gaps on rigid substrates. ECIS experiments are commonly performed without accounting for physiologically or pathologically relevant hydrostatic pressure across the endothelium nor are the influence of shear stress and cyclic stretch on endothelial barrier properties taken into

account. Even though the importance of such mechanical loads on endothelial properties has already been established in the early 90's [35,124,53,23], comparably few techniques have been described that actually include distinct mechanical forces in their experimental systems, as is nicely reviewed by Wegener and Seebach [114,28]. For example, ECIS electrodes have been introduced in laminar flow channels or cone and plate rheological systems [89,28]. Especially when it comes to studying the effect of short-lived rises in the local concentration of certain agonist, accounting for hydrodynamic flow can be an important aspect, as flow systems might help to understand the influence blood circulation on inflammatory agonist clearance and associated dynamics of endothelial barrier recovery after agonist washout. Taken together, in order to achieve a more accurate transferability of in vitro generated data to the physiological situation developments in these directions will be absolutely essential.

Acknowledgements

This work was partially supported by a postdoctoral fellowship from Applied Biophysics Inc. to J.S. and by grants R01HL097111 and R01 HL123364 from the NIH, and grant 14GRNT18880008 from the American Heart Association to M.T.; and partially by grant R01HL095566 from the NIH to K.M.

Non-standard Abbreviations and Acronyms

AC	Alternating Current
BBB	Blood Brain Barrier
DC	Direct Current
ECIS	Electric Cell-Substrate Impedance Sensing
FITC	Fluorescein-Isothiocyanate
GPCR	G-protein coupled receptor
HDMEC	Human dermal microvascular endothelial cells
His	Histamine
HUVEC	Human umbilical vein endothelial cells
ITO	Indium tinn oxide
RVSMC	Rat vascular smooth muscle cells
S1P	Sphingosine-1-Phosphate
TEER	Transendothelial (/Epithelial) electrical resistance
Thr	Thrombin
8W1E	8 wells, 1 electrode per well (1 working electrode / 1 counter electrode)
8W10E	8 wells, 10 electrodes per well (working electrode consisting of 10 small electrodes / 1 counter electrode)
8W10E+	8 wells, 40 electrodes per well (40 electrodes distributed on interdigitated finger pattern)

References

1. Adam AP, Sharenko AL, Pumiglia K, Vincent PA. Src-induced tyrosine phosphorylation of VE-cadherin is not sufficient to decrease barrier function of endothelial monolayers. The Journal of biological chemistry. 2010; 285(10):7045–7055. doi:10.1074/jbc.M109.079277. [PubMed: 20048167]
2. Aman J, van Bezu J, Damanafshan A, Huveneers S, Eringa EC, Vogel SM, Groeneveld AB, Vonk Noordegraaf A, van Hinsbergh VW, van Nieuw Amerongen GP. Effective treatment of edema and endothelial barrier dysfunction with imatinib. Circulation. 2012; 126(23):2728–2738. doi:10.1161/CIRCULATIONAHA.112.134304. [PubMed: 23099479]
3. Anderson JM, Van Itallie CM. Physiology and function of the tight junction. Cold Spring Harbor perspectives in biology. 2009; 1(2):a002584. doi:10.1101/cshperspect.a002584. [PubMed: 20066090]
4. Artus C, Glacial F, Ganeshamoorthy K, Ziegler N, Godet M, Guilbert T, Liebner S, Couraud PO. The Wnt/planar cell polarity signaling pathway contributes to the integrity of tight junctions in brain endothelial cells. Journal of cerebral blood flow and metabolism : official journal of the International Society of Cerebral Blood Flow and Metabolism. 2014; 34(3):433–440. doi:10.1038/jcbfm.2013.213.
5. Atienza JM, Yu N, Wang X, Xu X, Abassi Y. Label-free and real-time cell-based kinase assay for screening selective and potent receptor tyrosine kinase inhibitors using microelectronic sensor array. Journal of biomolecular screening. 2006; 11(6):634–643. doi:10.1177/1087057106289334. [PubMed: 16858006]
6. Atienza JM, Zhu J, Wang X, Xu X, Abassi Y. Dynamic monitoring of cell adhesion and spreading on microelectronic sensor arrays. Journal of biomolecular screening. 2005; 10(8):795–805. doi:10.1177/1087057105279635. [PubMed: 16234347]
7. Bagnaninchi PO, Drummond N. Real-time label-free monitoring of adipose-derived stem cell differentiation with electric cell-substrate impedance sensing. Proceedings of the National Academy of Sciences of the United States of America. 2011; 108(16):6462–6467. doi:10.1073/pnas.1018260108. [PubMed: 21464296]
8. Barsoukov, E.; Macdonald, JR. Impedance Spectroscopy: Theory, Experiment, and Applications. John Wiley & Sons, Hoboken; New Jersey, USA: 2005.
9. Bazzoni G. Endothelial tight junctions: permeable barriers of the vessel wall. Thrombosis and haemostasis. 2006; 95(1):36–42. [PubMed: 16543959]
10. Becker PM, Verin AD, Booth MA, Liu F, Birukova A, Garcia JG. Differential regulation of diverse physiological responses to VEGF in pulmonary endothelial cells. American journal of physiology Lung cellular and molecular physiology. 2001; 281(6):L1500–1511. [PubMed: 11704547]
11. Becker PM, Waltenberger J, Yachechko R, Mirzapoiazova T, Sham JS, Lee CG, Elias JA, Verin AD. Neuropilin-1 regulates vascular endothelial growth factor-mediated endothelial permeability. Circulation research. 2005; 96(12):1257–1265. doi:10.1161/01.RES.0000171756.13554.49. [PubMed: 15920019]
12. Benson K, Cramer S, Galla HJ. Impedance-based cell monitoring: barrier properties and beyond. Fluids and barriers of the CNS. 2013; 10(1):5. doi:10.1186/2045-8118-10-5. [PubMed: 23305242]
13. Bernas MJ, Cardoso FL, Daley SK, Weinand ME, Campos AR, Ferreira AJ, Hoying JB, Witte MH, Brites D, Persidsky Y, Ramirez SH, Brito MA. Establishment of primary cultures of human brain microvascular endothelial cells to provide an in vitro cellular model of the blood-brain barrier. Nature protocols. 2010; 5(7):1265–1272. doi:10.1038/nprot.2010.76. [PubMed: 20595955]
14. Birukova AA, Cokic I, Moldobaeva N, Birukov KG. Paxillin is involved in the differential regulation of endothelial barrier by HGF and VEGF. American journal of respiratory cell and molecular biology. 2009; 40(1):99–107. doi:10.1165/rcmb.2008-0099OC. [PubMed: 18664639]
15. Bogatcheva NV, Zemskova MA, Kovalenkov Y, Poirier C, Verin AD. Molecular mechanisms mediating protective effect of cAMP on lipopolysaccharide (LPS)-induced human lung microvascular endothelial cells (HLMVEC) hyperpermeability. Journal of cellular physiology. 2009; 221(3):750–759. doi:10.1002/jcp.21913. [PubMed: 19725051]

16. Bogatcheva NV, Zemskova MA, Poirier C, Mirzapoiazova T, Kolosova I, Bresnick AR, Verin AD. The suppression of myosin light chain (MLC) phosphorylation during the response to lipopolysaccharide (LPS): beneficial or detrimental to endothelial barrier? Journal of cellular physiology. 2011; 226(12):3132–3146. doi:10.1002/jcp.22669. [PubMed: 21302311]
17. Cecchelli R, Aday S, Sevin E, Almeida C, Culot M, Dehouck L, Coisne C, Engelhardt B, Dehouck MP, Ferreira L. A stable and reproducible human blood-brain barrier model derived from hematopoietic stem cells. PloS one. 2014; 9(6):e99733. doi:10.1371/journal.pone.0099733. [PubMed: 24936790]
18. Chatterjee A, Snead C, Yetik-Anacak G, Antonova G, Zeng J, Catravas JD. Heat shock protein 90 inhibitors attenuate LPS-induced endothelial hyperpermeability. American journal of physiology Lung cellular and molecular physiology. 2008; 294(4):L755–763. doi:10.1152/ajplung.00350.2007. [PubMed: 18245267]
19. Chen XL, Nam JO, Jean C, Lawson C, Walsh CT, Goka E, Lim ST, Tomar A, Tancioni I, Uryu S, Guan JL, Acevedo LM, Weis SM, Cheresh DA, Schlaepfer DD. VEGF-induced vascular permeability is mediated by FAK. Developmental cell. 2012; 22(1):146–157. doi:10.1016/j.devcel.2011.11.002. [PubMed: 22264731]
20. Cohen-Kashi Malina K, Cooper I, Teichberg VI. Closing the gap between the in-vivo and in-vitro blood-brain barrier tightness. Brain research. 2009; 1284:12–21. doi:10.1016/j.brainres.2009.05.072. [PubMed: 19501061]
21. Cooper JA, Del Vecchio PJ, Minnear FL, Burhop KE, Selig WM, Garcia JG, Malik AB. Measurement of albumin permeability across endothelial monolayers in vitro. Journal of applied physiology. 1987; 62(3):1076–1083. [PubMed: 3571065]
22. Daniels BP, Cruz-Orengo L, Pasieka TJ, Couraud PO, Romero IA, Weksler B, Cooper JA, Doering TL, Klein RS. Immortalized human cerebral microvascular endothelial cells maintain the properties of primary cells in an in vitro model of immune migration across the blood brain barrier. Journal of neuroscience methods. 2013; 212(1):173–179. doi:10.1016/j.jneumeth.2012.10.001. [PubMed: 23068604]
23. Davies PF, Remuzzi A, Gordon EJ, Dewey CF Jr. Gimbrone MA Jr. Turbulent fluid shear stress induces vascular endothelial cell turnover in vitro. Proceedings of the National Academy of Sciences of the United States of America. 1986; 83(7):2114–2117. [PubMed: 3457378]
24. Davis GE, Senger DR. Endothelial extracellular matrix: biosynthesis, remodeling, and functions during vascular morphogenesis and neovessel stabilization. Circulation research. 2005; 97(11):1093–1107. doi:10.1161/01.RES.0000191547.64391.e3. [PubMed: 16306453]
25. De Blasio BF, Laane M, Walmann T, Giaever I. Combining optical and electrical impedance techniques for quantitative measurement of confluence in MDCK-I cell cultures. BioTechniques. 2004; 36(4):650–654. 656, 658. passim. [PubMed: 15088383]
26. de Vries HE, Blom-Roosemalen MC, de Boer AG, van Berkel TJ, Breimer DD, Kuiper J. Effect of endotoxin on permeability of bovine cerebral endothelial cell layers in vitro. The Journal of pharmacology and experimental therapeutics. 1996; 277(3):1418–1423. [PubMed: 8667205]
27. DeMaio L, Tarbell JM, Scaduto RC Jr. Gardner TW, Antonetti DA. A transmural pressure gradient induces mechanical and biological adaptive responses in endothelial cells. American journal of physiology Heart and circulatory physiology. 2004; 286(2):H731–741. doi:10.1152/ajpheart.00427.2003. [PubMed: 14527936]
28. DePaola N, Phelps JE, Florez L, Keese CR, Minnear FL, Giaever I, Vincent P. Electrical impedance of cultured endothelium under fluid flow. Annals of biomedical engineering. 2001; 29(8):648–656. [PubMed: 11556721]
29. Dewi BE, Takasaki T, Kurane I. In vitro assessment of human endothelial cell permeability: effects of inflammatory cytokines and dengue virus infection. Journal of virological methods. 2004; 121(2):171–180. doi:10.1016/j.jviromet.2004.06.013. [PubMed: 15381354]
30. Dubrovskyi O, Birukova AA, Birukov KG. Measurement of local permeability at subcellular level in cell models of agonist- and ventilator-induced lung injury. Laboratory investigation; a journal of technical methods and pathology. 2013; 93(2):254–263. doi:10.1038/labinvest.2012.159.
31. Ehret R, Baumann W, Brischwein M, Schwinde A, Stegbauer K, Wolf B. Monitoring of cellular behaviour by impedance measurements on interdigitated electrode structures. Biosensors & bioelectronics. 1997; 12(1):29–41. [PubMed: 8976050]

32. Ehret R, Baumann W, Brischwein M, Schwinde A, Wolf B. On-line control of cellular adhesion with impedance measurements using interdigitated electrode structures. Medical & biological engineering & computing. 1998; 36(3):365–370. [PubMed: 9747579]
33. Estrada R, Zeng Q, Lu H, Sarojini H, Lee JF, Mathis SP, Sanchez T, Wang E, Kontos CD, Lin CY, Hla T, Haribabu B, Lee MJ. Up-regulating sphingosine 1-phosphate receptor-2 signaling impairs chemotactic, wound-healing, and morphogenetic responses in senescent endothelial cells. The Journal of biological chemistry. 2008; 283(44):30363–30375. doi:10.1074/jbc.M804392200. [PubMed: 18765664]
34. Faurobert E, Rome C, Lisowska J, Manet-Dupe S, Boulday G, Malbouyres M, Balland M, Bouin AP, Keramidas M, Bouvard D, Coll JL, Ruggiero F, Tournier-Lasserve E, Albiges-Rizo C. CCM1-ICAP-1 complex controls beta1 integrin-dependent endothelial contractility and fibronectin remodeling. The Journal of cell biology. 2013; 202(3):545–561. doi:10.1083/jcb.201303044. [PubMed: 23918940]
35. Franke RP, Grafe M, Schnittler H, Seiffge D, Mittermayer C, Drenckhahn D. Induction of human vascular endothelial stress fibres by fluid shear stress. Nature. 1984; 307(5952):648–649. [PubMed: 6537993]
36. Garcia JG, Liu F, Verin AD, Birukova A, Dechert MA, Gerthoffer WT, Bamberg JR, English D. Sphingosine 1-phosphate promotes endothelial cell barrier integrity by Edg-dependent cytoskeletal rearrangement. The Journal of clinical investigation. 2001; 108(5):689–701. doi:10.1172/JCI12450. [PubMed: 11544274]
37. Garcia JG, Siflinger-Birnboim A, Bizios R, Del Vecchio PJ, Fenton JW 2nd, Malik AB. Thrombin-induced increase in albumin permeability across the endothelium. Journal of cellular physiology. 1986; 128(1):96–104. doi:10.1002/jcp.1041280115. [PubMed: 3722274]
38. Giaever I, Keese CR. Monitoring fibroblast behavior in tissue culture with an applied electric field. Proceedings of the National Academy of Sciences of the United States of America. 1984; 81(12):3761–3764. [PubMed: 6587391]
39. Giaever I, Keese CR. Micromotion of mammalian cells measured electrically. Proceedings of the National Academy of Sciences of the United States of America. 1991; 88(17):7896–7900. [PubMed: 1881923]
40. Heijink IH, van Oosterhout A, Kapus A. Epidermal growth factor receptor signalling contributes to house dust mite-induced epithelial barrier dysfunction. The European respiratory journal. 2010; 36(5):1016–1026. doi:10.1183/09031936.00125809. [PubMed: 20351035]
41. Herron CR, Lowery AM, Hollister PR, Reynolds AB, Vincent PA. p120 regulates endothelial permeability independently of its NH2 terminus and Rho binding. American journal of physiology Heart and circulatory physiology. 2011; 300(1):H36–48. doi:10.1152/ajpheart.00812.2010. [PubMed: 20971762]
42. Hofmann U, Michaelis S, Winckler T, Wegener J, Feller KH. A whole-cell biosensor as in vitro alternative to skin irritation tests. Biosensors & bioelectronics. 2013; 39(1):156–162. doi:10.1016/j.bios.2012.07.075. [PubMed: 22917920]
43. Hoheisel D, Nitz T, Franke H, Wegener J, Hakvoort A, Tilling T, Galla HJ. Hydrocortisone reinforces the blood-brain barrier in a serum-free culture system. Biochem Biophys Res Commun. 1998; 224(1):312–316.
44. Janshoff A, Wegener J, Sieber M, Galla HJ. Double-mode impedance analysis of epithelial cell monolyers cultured on shear wave resonators. Eur Biophys J. 1996; (25):93–103. [PubMed: 9035374]
45. Karczewski J, Troost FJ, Konings I, Dekker J, Kleerebezem M, Brummer RJ, Wells JM. Regulation of human epithelial tight junction proteins by Lactobacillus plantarum in vivo and protective effects on the epithelial barrier. American journal of physiology Gastrointestinal and liver physiology. 2010; 298(6):G851–859. doi:10.1152/ajpgi.00327.2009. [PubMed: 20224007]
46. Keese CR, Bhawe K, Wegener J, Giaever I. Real-time impedance assay to follow the invasive activities of metastatic cells in culture. BioTechniques. 2002; 33(4):842–844. 846, 848–850. [PubMed: 12398193]
47. Keese CR, Wegener J, Walker SR, Giaever I. Electrical wound-healing assay for cells in vitro. Proceedings of the National Academy of Sciences of the United States of America. 2004; 101(6):1554–1559. doi:10.1073/pnas.0307588100. [PubMed: 14747654]

48. Kim YV, Di Cello F, Hillaire CS, Kim KS. Differential Ca2+ signaling by thrombin and protease-activated receptor-1-activating peptide in human brain microvascular endothelial cells. American journal of physiology Cell physiology. 2004; 286(1):C31–42. doi:10.1152/ajpcell.00157.2003. [PubMed: 12944324]

49. Kobayashi K, Tsubosaka Y, Hori M, Narumiya S, Ozaki H, Murata T. Prostaglandin D2-DP signaling promotes endothelial barrier function via the cAMP/PKA/Tiam1/Rac1 pathway. Arteriosclerosis, thrombosis, and vascular biology. 2013; 33(3):565–571. doi:10.1161/ATVBAHA.112.300993.

50. Kobayashi N, Nishi T, Hirata T, Kihara A, Sano T, Igarashi Y, Yamaguchi A. Sphingosine 1-phosphate is released from the cytosol of rat platelets in a carrier-mediated manner. Journal of lipid research. 2006; 47(3):614–621. doi:10.1194/jlr.M500468-JLR200. [PubMed: 16371645]

51. Konya V, Ullen A, Kampitsch N, Theiler A, Philipose S, Parzmair GP, Marsche G, Peskar BA, Schuligoi R, Sattler W, Heinemann A. Endothelial E-type prostanoid 4 receptors promote barrier function and inhibit neutrophil trafficking. The Journal of allergy and clinical immunology. 2013; 131(2):532–540. e531–532. doi:10.1016/j.jaci.2012.05.008. [PubMed: 22704539]

52. Kuo YC, Su CH, Liu CY, Chen TH, Chen CP, Wang HS. Transforming growth factor-beta induces CD44 cleavage that promotes migration of MDA-MB-435s cells through the up-regulation of membrane type 1-matrix metalloproteinase. International journal of cancer Journal international du cancer. 2009; 124(11):2568–2576. doi:10.1002/ijc.24263. [PubMed: 19243022]

53. Lamontagne D, Pohl U, Busse R. Mechanical deformation of vessel wall and shear stress determine the basal release of endothelium-derived relaxing factor in the intact rabbit coronary vascular bed. Circulation research. 1992; 70(1):123–130. [PubMed: 1345777]

54. Lien CF, Mohanta SK, Frontczak-Baniewicz M, Swinny JD, Zablocka B, Gorecki DC. Absence of glial alpha-dystrobrevin causes abnormalities of the blood-brain barrier and progressive brain edema. The Journal of biological chemistry. 2012; 287(49):41374–41385. doi:10.1074/jbc.M112.400044. [PubMed: 23043099]

55. Liu Q, Yu J, Xiao L, Tang JC, Zhang Y, Wang P, Yang M. Impedance studies of bio-behavior and chemosensitivity of cancer cells by micro-electrode arrays. Biosensors & Bioelectronics. 2009; 24(5):1305–1310. doi:S0956-5663(08)00398-9 [pii] 10.1016/j.bios.2008.07.044. [PubMed: 18783935]

56. Lo CM, Keese CR, Giaever I. Monitoring motion of confluent cells in tissue culture. Experimental cell research. 1993; 204(1):102–109. doi:10.1006/excr.1993.1014. [PubMed: 8416788]

57. Lo CM, Keese CR, Giaever I. pH changes in pulsed CO2 incubators cause periodic changes in cell morphology. Experimental cell research. 1994; 213(2):391–397. doi:10.1006/excr.1994.1214. [PubMed: 8050495]

58. Lo CM, Keese CR, Giaever I. Cell-substrate contact: another factor may influence transepithelial electrical resistance of cell layers cultured on permeable filters. Experimental cell. 1999; 250(2):576–580. doi:10.1006/excr.1999.4538.

59. Lorenowicz MJ, Fernandez-Borja M, Kooistra MR, Bos JL, Hordijk PL. PKA and Epac1 regulate endothelial integrity and migration through parallel and independent pathways. European journal of cell biology. 2008; 87(10):779–792. doi:10.1016/j.ejcb.2008.05.004. [PubMed: 18635287]

60. Lovelady DC, Friedman J, Patel S, Rabson DA, Lo CM. Detecting effects of low levels of cytochalasin B in 3T3 fibroblast cultures by analysis of electrical noise obtained from cellular micromotion. Biosensors & bioelectronics. 2009; 24(7):2250–2254. doi:10.1016/j.bios.2008.09.033. [PubMed: 19026529]

61. Luissint AC, Federici C, Guillonneau F, Chretien F, Camoin L, Glacial F, Ganeshamoorthy K, Couraud PO. Guanine nucleotide-binding protein Galphai2: a new partner of claudin-5 that regulates tight junction integrity in human brain endothelial cells. Journal of cerebral blood flow and metabolism : official journal of the International Society of Cerebral Blood Flow and Metabolism. 2012; 32(5):860–873. doi:10.1038/jcbfm.2011.202.

62. Lvovich, VF. Impedance Spectroscopy: Applications to Electrochemical and DielectricPhenomena. John Wiley & Sons; Hoboken, New Jersey, USA: 2012.

63. Lynch JJ, Ferro TJ, Blumenstock FA, Brockenauer AM, Malik AB. Increased endothelial albumin permeability mediated by protein kinase C activation. The Journal of clinical investigation. 1990; 85(6):1991–1998. doi:10.1172/JCI114663. [PubMed: 2347922]

64. McAdams ET, Lackermeier A, McLaughlin JA, Macken D, Jossinet J. The linear and nonlinear electrical properties of the electrode-electrolyte interface. Biosensors & bioelectronics. 1995; 10:76–74.

65. McLaughlin JN, Shen L, Holinstat M, Brooks JD, Dibenedetto E, Hamm HE. Functional selectivity of G protein signaling by agonist peptides and thrombin for the protease-activated receptor-1. The Journal of biological chemistry. 2005; 280(26):25048–25059. doi:10.1074/jbc.M414090200. [PubMed: 15878870]

66. Mehta D, Malik AB. Signaling mechanisms regulating endothelial permeability. Physiological reviews. 2006; 86(1):279–367. doi:10.1152/physrev.00012.2005. [PubMed: 16371600]

67. Michaelis S, Rommel CE, Endell J, Goring P, Wehrsporn R, Steinem C, Janshoff A, Galla HJ, Wegener J. Macroporous silicon chips for laterally resolved, multi-parametric analysis of epithelial barrier function. Lab Chip. 2013; (12):2329–2336.

68. Michaelis S, Wegener J, Robelek R. Label-free monitoring of cell-based assays: combining impedance analysis with SPR for multiparametric cell profiling. Biosens Bioelectron. 2013; (49): 63–70. [PubMed: 23711901]

69. Michel CC. Transport of macromolecules through microvascular walls. Cardiovascular research. 1996; 32(4):644–653. [PubMed: 8915183]

70. Monaghan-Benson E, Wittchen ES. In vitro analyses of endothelial cell permeability. Methods in molecular biology. 2011; 763:281–290. doi:10.1007/978-1-61779-191-8_19. [PubMed: 21874459]

71. Moore E, Rawley O, Wood T, Galvin P. Monitoring of cell growth in vitro using biochips packaged with indium tin oxide sensors. Sensors and Actators B-Chemical. 2009; (139):187–193.

72. Moy AB, Blackwell K, Kamath A. Differential effects of histamine and thrombin on endothelial barrier function through actin-myosin tension. American journal of physiology Heart and circulatory physiology. 2002; 282(1):H21–29. [PubMed: 11748043]

73. Murata N, Sato K, Kon J, Tomura H, Yanagita M, Kuwabara A, Ui M, Okajima F. Interaction of sphingosine 1-phosphate with plasma components, including lipoproteins, regulates the lipid receptor-mediated actions. The Biochemical journal. 2000; 352(Pt 3):809–815. [PubMed: 11104690]

74. Murata T, Aritake K, Tsubosaka Y, Maruyama T, Nakagawa T, Hori M, Hirai H, Nakamura M, Narumiya S, Urade Y, Ozaki H. Anti-inflammatory role of PGD2 in acute lung inflammation and therapeutic application of its signal enhancement. Proceedings of the National Academy of Sciences of the United States of America. 2013; 110(13):5205–5210. doi:10.1073/pnas.1218091110. [PubMed: 23479612]

75. Mycielska ME, Djamgoz MB. Cellular mechanisms of direct-current electric field effects: galvanotaxis and metastatic disease. Journal of cell science. 2004; 117(Pt 9):1631–1639. doi:10.1242/jcs.01125. [PubMed: 15075225]

76. Nakagawa S, Deli MA, Kawaguchi H, Shimizudani T, Shimono T, Kittel A, Tanaka K, Niwa M. A new blood-brain barrier model using primary rat brain endothelial cells, pericytes and astrocytes. Neurochemistry international. 2009; 54(3-4):253–263. doi:10.1016/j.neuint.2008.12.002. [PubMed: 19111869]

77. Panke O, Weigel W, Schmidt S, Steude A, Robitzki AA. A cell-based impedance assay for monitoring transient receptor potential (TRP) ion channel activity. Biosensors & bioelectronics. 2011; 26(5):2376–2382. doi:10.1016/j.bios.2010.10.015. [PubMed: 21051219]

78. Paolinelli R, Corada M, Ferrarini L, Devraj K, Artus C, Czupalla CJ, Rudini N, Maddaluno L, Papa E, Engelhardt B, Couraud PO, Liebner S, Dejana E. Wnt activation of immortalized brain endothelial cells as a tool for generating a standardized model of the blood brain barrier in vitro. PloS one. 2013; 8(8):e70233. doi:10.1371/journal.pone.0070233. [PubMed: 23940549]

79. Parker JC, Stevens T, Randall J, Weber DS, King JA. Hydraulic conductance of pulmonary microvascular and macrovascular endothelial cell monolayers. American journal of physiology Lung cellular and molecular physiology. 2006; 291(1):L30–37. doi:10.1152/ajplung.00317.2005. [PubMed: 16760315]

80. Rahman ARA, Lo CM, Bhansali S. A micro-electrode array biosensor for impedance spectroscopy of human umbilical vein endothelial cells. Sensors & Actuators B-Chemical. 2006; 118:115–120.

81. Ramirez-Icaza G, Mohammed KA, Nasreen N, Van Horn RD, Hardwick JA, Sanders KL, Tian J, Ramirez-Icaza C, Johnson MT, Antony VB. Th2 cytokines IL-4 and IL-13 downregulate paxillin expression in bronchial airway epithelial cells. Journal of clinical immunology. 2004; 24(4):426–434. doi:10.1023/B:JOCI.0000029111.27168.c6. [PubMed: 15163899]
82. Rehder D, Iden S, Nasdala I, Wegener J, Brickwedde MK, Vestweber D, Ebnet K. Junctional adhesion molecule-a participates in the formation of apico-basal polarity through different domains. Experimental cell research. 2006; 312(17):3389–3403. doi:10.1016/j.yexcr.2006.07.004. [PubMed: 16919624]
83. Riethmuller C, Jungmann P, Wegener J, Oberleithner H. Bradykinin shifts endothelial fluid passage from para- to transcellular routes. Pflugers Archiv : European journal of physiology. 2006; 453(2):157–165. doi:10.1007/s00424-006-0121-2. [PubMed: 17047985]
84. Rosen H, Stevens RC, Hanson M, Roberts E, Oldstone MB. Sphingosine-1-phosphate and its receptors: structure, signaling, and influence. Annual review of biochemistry. 2013; 82:637–662. doi:10.1146/annurev-biochem-062411-130916.
85. Schiller KR, Maniak PJ, O'Grady SM. Cystic fibrosis transmembrane conductance regulator is involved in airway epithelial wound repair. American journal of physiology Cell physiology. 2010; 299(5):C912–921. doi:10.1152/ajpcell.00215.2010. [PubMed: 20686068]
86. Schlegel N, Waschke J. Impaired cAMP and Rac 1 signaling contribute to TNF-alpha-induced endothelial barrier breakdown in microvascular endothelium. Microcirculation. 2009; 16(6):521–533. doi:10.1080/10739680902967427. [PubMed: 19504398]
87. Schneider D, Tarantola M, Janshoff A. Dynamics of TGF-beta induced epithelial-tomesenchymal transition monitored by electric cell-substrate impedance sensing. Biochimica et biophysica acta. 2011; 1813(12):2099–2107. doi:10.1016/j.bbamcr.2011.07.016. [PubMed: 21839117]
88. Schnoor M, Lai FP, Zarbock A, Klaver R, Polaschegg C, Schulte D, Weich HA, Oelkers JM, Rottner K, Vestweber D. Cortactin deficiency is associated with reduced neutrophil recruitment but increased vascular permeability in vivo. The Journal of experimental medicine. 2011; 208(8):1721–1735. doi:10.1084/jem.20101920. [PubMed: 21788407]
89. Seebach J, Dieterich P, Luo F, Schillers H, Vestweber D, Oberleithner H, Galla HJ, Schnittler HJ. Endothelial barrier function under laminar fluid shear stress. Laboratory investigation; a journal of technical methods and pathology. 2000; 80(12):1819–1831.
90. Shinde AV, Motiani RK, Zhang X, Abdullaev IF, Adam AP, Gonzalez-Cobos JC, Zhang W, Matrougui K, Vincent PA, Trebak M. STIM1 controls endothelial barrier function independently of Orai1 and Ca2+ entry. Science signaling. 2013; 6(267):ra18. doi:10.1126/scisignal.2003425. [PubMed: 23512989]
91. Shivanna M, Rajashekhar G, Srinivas SP. Barrier dysfunction of the corneal endothelium in response to TNF-alpha: role of p38 MAP kinase. Investigative ophthalmology & visual science. 2010; 51(3):1575–1582. doi:10.1167/iovs.09-4343. [PubMed: 19797215]
92. Solly K, Wang X, Xu X, Strulovici B, Zheng W. Application of real-time cell electronic sensing (RT-CES) technology to cell-based assays. Assay and drug development technologies. 2004; 2(4):363–372. doi:10.1089/1540658041850544. [PubMed: 15357917]
93. Spindler V, Peter D, Harms GS, Asan E, Waschke J. Ultrastructural analysis reveals cAMP-dependent enhancement of microvascular endothelial barrier functions via Rac1-mediated reorganization of intercellular junctions. The American journal of pathology. 2011; 178(5):2424–2436. doi:10.1016/j.ajpath.2011.01.014. [PubMed: 21457935]
94. Stamatovic SM, Keep RF, Andjelkovic AV. Brain endothelial cell-cell junctions: how to “open” the blood brain barrier. Current neuropharmacology. 2008; 6(3):179–192. doi:10.2174/157015908785777210. [PubMed: 19506719]
95. Stolwijk JA, Hartmann C, Balani P, Albermann S, Keese CR, Giaever I, Wegener J. Impedance analysis of adherent cells after in situ electroporation: non-invasive monitoring during intracellular manipulations. Biosens Bioelectron. 2011; (26):4720–4727. [PubMed: 21684144]
96. Sun M, Fu H, Cheng H, Cao Q, Zhao Y, Mou X, Zhang X, Liu X, Ke Y. A dynamic real-time method for monitoring epithelial barrier function in vitro. Analytical biochemistry. 2012; 425(2):96–103. doi:10.1016/j.ab.2012.03.010. [PubMed: 22449498]

97. Szulcek R, Beckers CM, Hodzic J, de Wit J, Chen Z, Grob T, Musters RJ, Minshall RD, van Hinsbergh VW, van Nieuw Amerongen GP. Localized RhoA GTPase activity regulates dynamics of endothelial monolayer integrity. Cardiovascular research. 2013; 99(3):471–482. doi: 10.1093/cvr/cvt075. [PubMed: 23536606]

98. Szulcek R, Bogaard HJ, van Nieuw Amerongen GP. Electric cell-substrate impedance sensing for the quantification of endothelial proliferation, barrier function, and motility. Journal of visualized experiments : JoVE. 2014; (85) doi:10.3791/51300.

99. Tang VW, Goodenough DA. Paracellular ion channel at the tight junction. Biophysical journal. 2003; 84(3):1660–1673. doi:10.1016/S0006-3495(03)74975-3. [PubMed: 12609869]

100. Tarantola M, Marel AK, Sunnick E, Adam H, Wegener J, Janshoff A. Dynamics of human cancer cell lines monitored by electrical and acoustic fluctuation analysis. Integrative biology : quantitative biosciences from nano to macro. 2010; 2(2-3):139–150. doi:10.1039/b920815a. [PubMed: 20473392]

101. ten Klooster JP, Jaffer ZM, Chernoff J, Hordijk PL. Targeting and activation of Rac1 are mediated by the exchange factor beta-Pix. The Journal of cell biology. 2006; 172(5):759–769. doi:10.1083/jcb.200509096. [PubMed: 16492808]

102. Tiruppathi C, Malik AB, Del Vecchio PJ, Keese CR, Giaever I. Electrical method for detection of endothelial cell shape change in real time: assessment of endothelial barrier function. Proceedings of the National Academy of Sciences of the United States of America. 1992; 89(17): 7919–7923. [PubMed: 1518814]

103. Turner MR. Flows of liquid and electrical current through monolayers of cultured bovine arterial endothelium. The Journal of physiology. 1992; 449:1–20. [PubMed: 1522505]

104. Utoguchi N, Ikeda K, Saeki K, Oka N, Mizuguchi H, Kubo K, Nakagawa S, Nayumi T. Ascorbic acid stimulates barrier function of cultured endothelial cell monolayer. J Cell Physiol. 1995; 163(2):393–399. [PubMed: 7706381]

105. Van Itallie CM, Anderson JM. The role of claudins in determining paracellular charge selectivity. Proceedings of the American Thoracic Society. 2004; 1(1):38–41. doi:10.1513/pats.2306013. [PubMed: 16113410]

106. von Wedel-Parlow M, Schrot S, Lemmen J, Treeratanapiboon L, Wegener J, Galla HJ. Neutrophils cross the BBB primarily on transcellular pathways: an in vitro study. Brain research. 2011; 1367:62–76. doi:10.1016/j.brainres.2010.09.076. [PubMed: 20875807]

107. von Wedel-Parlow M, Wolte P, Galla HJ. Regulation of major efflux transporters under inflammatory conditions at the blood-brain barrier in vitro. Journal of neurochemistry. 2009; 111(1):111–118. doi:10.1111/j.1471-4159.2009.06305.x. [PubMed: 19656257]

108. Wallez Y, Huber P. Endothelial adherens and tight junctions in vascular homeostasis, inflammation and angiogenesis. Biochimica et biophysica acta. 2008; 1778(3):794–809. doi: 10.1016/j.bbamem.2007.09.003. [PubMed: 17961505]

109. Wang Y, Alexander JS. Analysis of endothelial barrier function in vitro. Methods in molecular biology. 2011; 763:253–264. doi:10.1007/978-1-61779-191-8_17. [PubMed: 21874457]

110. Wang Z, Ginnan R, Abdullaev IF, Trebak M, Vincent PA, Singer HA. Calcium/Calmodulin-dependent protein kinase II delta 6 (CaMKIIdelta6) and RhoA involvement in thrombin-induced endothelial barrier dysfunction. The Journal of biological chemistry. 2010; 285(28):21303–21312. doi:10.1074/jbc.M110.120790. [PubMed: 20442409]

111. Wegener J, Abrams D, Willenbrink W, Galla HJ, Janshoff A. Automated multi-well device to measure transepithelial electrical resistances under physiological conditions. BioTechniques. 2004; 37(4):590, 592–594, 596–597. [PubMed: 15517971]

112. Wegener J, Hakvoort A, Galla HJ. Barrier function of porcine choroid plexus epithelial cells is modulated by cAMP-dependent pathways in vitro. Brain research. 2000; 853(1):115–124. [PubMed: 10627315]

113. Wegener J, Keese CR, Giaever I. Electric cell-substrate impedance sensing (ECIS) as a noninvasive means to monitor the kinetics of cell spreading to artificial surfaces. Experimental cell research. 2000; 259(1):158–166. doi:10.1006/excr.2000.4919. [PubMed: 10942588]

114. Wegener J, Seebach J. Experimental tools to monitor the dynamics of endothelial barrier function: a survey of in vitro approaches. Cell and tissue research. 2014; 355(3):485–514. doi: 10.1007/s00441-014-1810-3. [PubMed: 24585359]
115. Weidenfeller C, Schrot S, Zozulya A, Galla HJ. Murine brain capillary endothelial cells exhibit improved barrier properties under the influence of hydrocortisone. Brain research. 2005; 1053(1-2):162–174. doi:10.1016/j.brainres.2005.06.049. [PubMed: 16040011]
116. Wilhelm I, Fazakas C, Krizbai IA. In vitro models of the blood-brain barrier. Acta neurobiologiae experimentalis. 2011; 71(1):113–128. [PubMed: 21499332]
117. Wilkerson BA, Grass GD, Wing SB, Argraves WS, Argraves KM. Sphingosine 1-phosphate (S1P) carrier-dependent regulation of endothelial barrier: high density lipoprotein (HDL)-S1P prolongs endothelial barrier enhancement as compared with albumin-S1P via effects on levels, trafficking, and signaling of S1P1. The Journal of biological chemistry. 2012; 287(53):44645–44653. doi:10.1074/jbc.M112.423426. [PubMed: 23135269]
118. Will C, Fromm M, Muller D. Claudin tight junction proteins: novel aspects in paracellular transport. Peritoneal dialysis international : journal of the International Society for Peritoneal Dialysis. 2008; 28(6):577–584. [PubMed: 18981384]
119. Wolf P, Rothermel A, Beck-Sickinger AG, Robitzki AA. Microelectrode chip based real time monitoring of vital MCF-7 mamma carcinoma cells by impedance spectroscopy. Biosensors & bioelectronics. 2008; 24(2):253–259. doi:10.1016/j.bios.2008.03.040. [PubMed: 18468883]
120. Xiao C, Lachance B, Sunahara G, Luong JH. Assessment of cytotoxicity using electric cell-substrate impedance sensing: concentration and time response function approach. Analytical chemistry. 2002; 74(22):5748–5753. [PubMed: 12463358]
121. Xiao C, Luong JH. On-line monitoring of cell growth and cytotoxicity using electric cell-substrate impedance sensing (ECIS). Biotechnology progress. 2003; 19(3):1000–1005. doi: 10.1021/bp025733x. [PubMed: 12790667]
122. Xu M, Waters CL, Hu C, Wysolmerski RB, Vincent PA, Minnear FL. Sphingosine 1-phosphate rapidly increases endothelial barrier function independently of VE-cadherin but requires cell spreading and Rho kinase. American journal of physiology Cell physiology. 2007; 293(4):C1309–1318. doi:10.1152/ajpcell.00014.2007. [PubMed: 17670896]
123. Yin F, Watsky MA. LPA and S1P increase corneal epithelial and endothelial cell transcellular resistance. Investigative ophthalmology & visual science. 2005; 46(6):1927–1933. doi:10.1167/iovs.04-1256. [PubMed: 15914605]
124. Yoshida Y, Okano M, Wang S, Kobayashi M, Kawasumi M, Hagiwara H, Mitsumata M. Hemodynamic-force-induced difference of interendothelial junctional complexes. Annals of the New York Academy of Sciences. 1995; 748:104–120. discussion 120-101. [PubMed: 7695160]
125. Yuan, SY.; Rigor, RR. Methods for Measuring Permeability.. In: Yuan, SY.; Rigor, RR., editors. Regulation of Endothelial Barrier Function. Morgan & Claypool Life Sciences; San Rafael (CA): 2010. 2010.

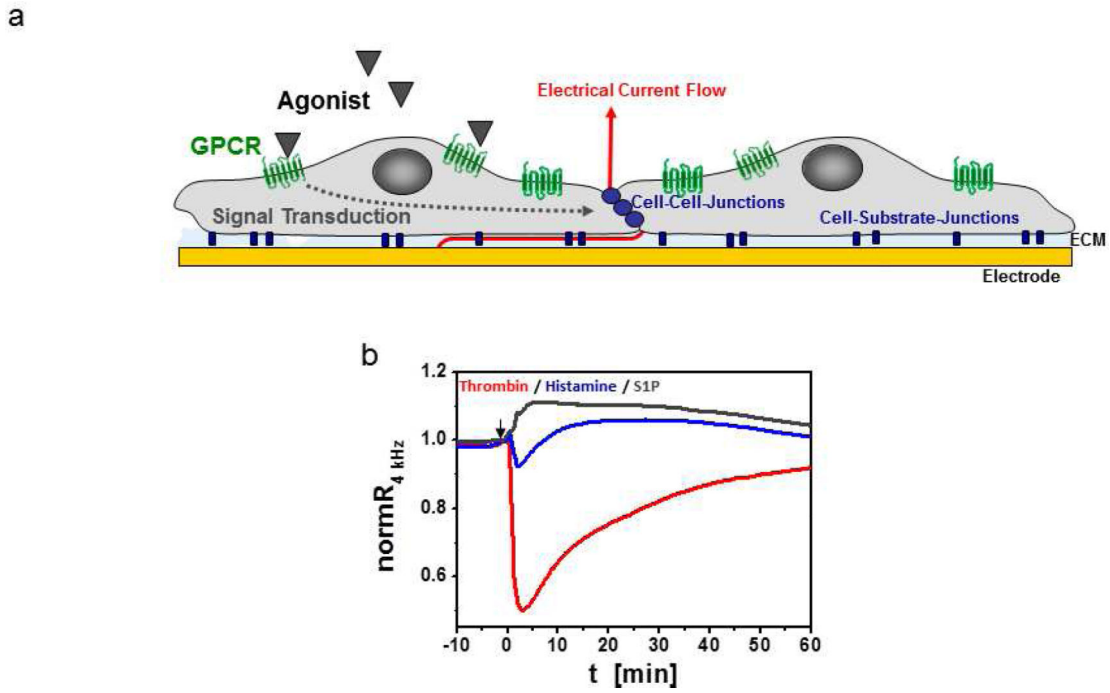

Fig. 1.

ECIS for monitoring of changes in endothelial barrier function upon GPCR stimulation. **a** Schematic illustration of endothelial cells on an ECIS electrode. Signal transduction after GPCR stimulation often results in changes in the cytoskeleton, at cell-cell and/or cell-substrate junctions. Resulting changes in the dimensions of the subcellular and intercellular cleft can be measured with ECIS as changes in alternating current flow at 4 kHz across the cell layer. ECM: Extracellular matrix. **b** Typicalresponse profiles of HDMEC cell layers after stimulation with either 5 nM thrombin (red trace), 10 μM histamine (blue trace) or 1 μM S1P (grey trace). Data were normalized to resistances before agonist addition. Absolute baseline values of respective cell layers before agonist addition were around 4000 for histamine and thrombin and 2200 for S1P.

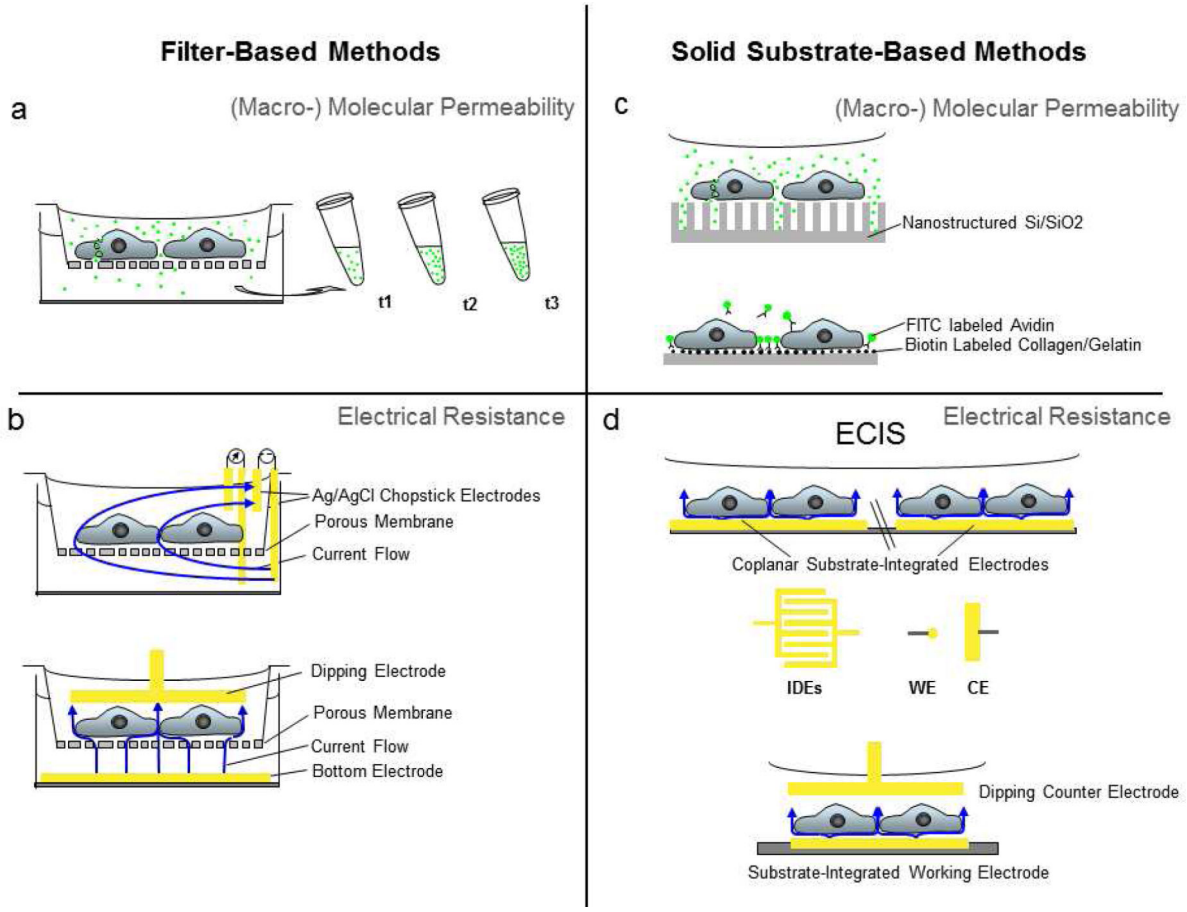

Fig. 2.

Overview of popular *in vitro* systems for study of barrier function using cultured endothelial cells.**a, b** Filter-based methods: Cultured endothelial cells are grown onto permeable filter supports to measure **a** passage of tracer molecules across an endothelial cell layer or **b** transendothelial electrical resistance (TEER) using a 4-electrode (upper panel) or 2-electrode setup (lower panel). Yellow bars indicate electrodes of conductive material (e.g. Ag, Au, stainless steel, platinum, indium tin oxide). Blue arrows indicate current flow, which is unidirectional for DC or bidirectional for AC signals (drawn unidirectionally for clarity). **c, d** Solid substrate based methods: **c** Recently developed techniques for molecular permeability using macroporous silicon that serve as microcuvettes (upper panel) or specific biotin/avidin interactions to immobilize tracer molecules at the site of molecule passage through the cell layer (lower panel). **d** Cells directly grown onto substrate-integrated electrodes are the basis for ECIS and related electrical techniques. Typically, substrate-integrated electrodes are in coplanar arrangement (upper setup). Note that the counter electrode (CE) is usually significantly larger than the working electrode (WE). In this setup the ECIS signal is dominated by changes that occur at the small working electrode. With the use of interdigitated electrodes (IDEs) with finger-like patterns, both electrodes contribute equally to the overall impedance signal. Alternatively, the counter electrode can be submersed into the culture medium approaching from the top (lower setup). Only the working electrode is substrate integrated. In this case the counter dipping electrode needs to

have an at least 500-fold bigger surface area to make its contribution to the measurement negligible.

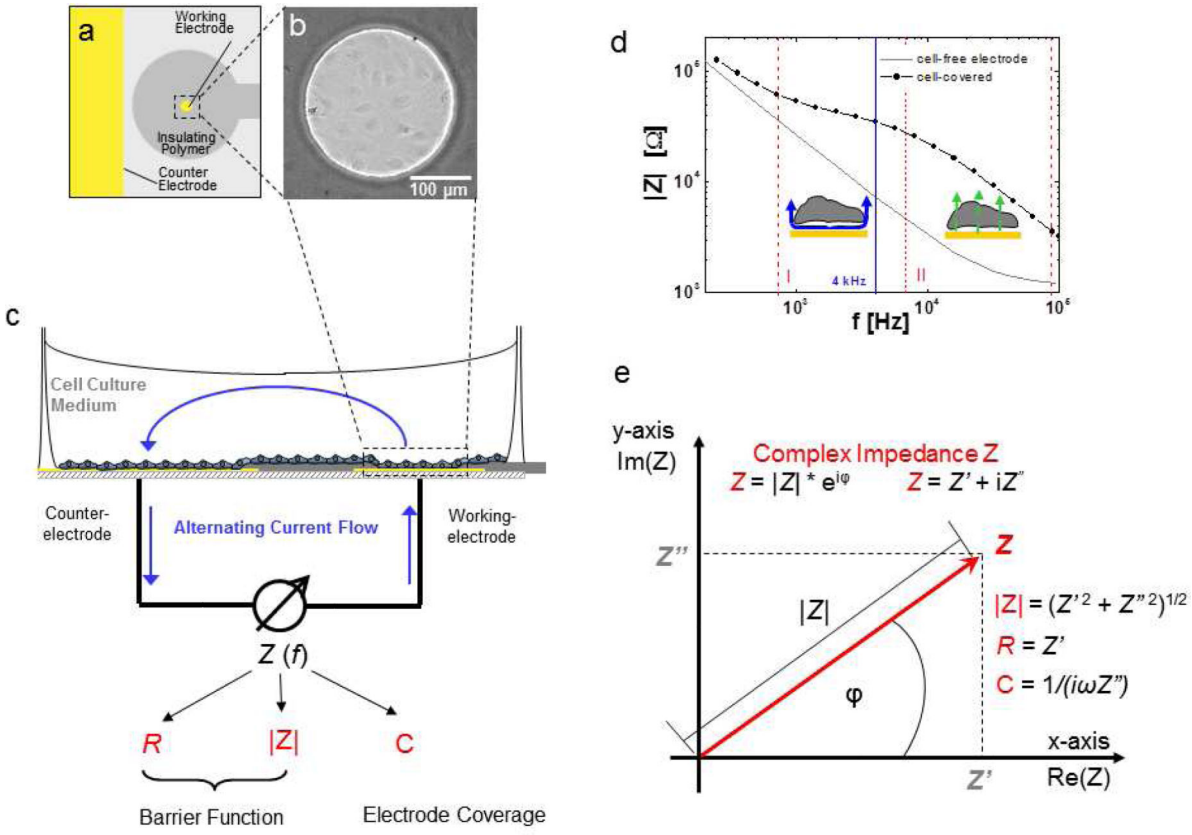

Fig. 3.

Principle of ECIS. **a** Schematic of co-planar two-electrode layout of one ECIS chamber viewed from top (yellow: gold electrode surfaces, grey: insulating polymer). **b** Phase contrast micrograph of an ECIS working electrode covered with HDMEC cells. **c** Schematic side view of ECIS chamber and principle of measurement. Electrical connection between the small working electrode (~ 5×10^{-4} cm^2) and the significantly larger counter electrode is provided by the cell culture medium. Blue arrows, drawn unidirectionally for clarity, indicate the alternating current flow. The complex impedance *Z* of the system is measured as a function of frequency and comprises information on resistive (*R*) as well as capacitive (*C*) behavior of the system. Impedance magnitude |Z|, Ohmic resistance *R* and capacitance *C* are used as typical monitoring parameters to measure cell behavior. **d** The frequency dependent behavior of a cell-free and cell-covered electrode presented in a so-called Bode diagram, reflecting the impedance increase due to the cell layer between ~ 10^3 – 10^5 Hz. For the system presented here, the signal is dominated by the paracellular cell layer resistance between about 10^3 – 10^4 Hz (section I delineated by dashed red lines) and is increasingly influenced by capacitive currents across the cell membranes between 10^4 – 10^5 Hz (section II delineated by dashed red lines). **e** The complex impedance *Z* can be graphically presented as a vector in a complex plane. Herein, the complex impedance *Z* is described by the length of the vector, its magnitude |*Z*|, which is the ratio of the amplitudes V_0 and I_0 according to Ohm's law, and the angle between the vector and the x-axis, which describes the frequency-dependent phase shift ϕ. As expressed in Cartesian coordinates, the x-axis (Real axis in complex plane) describes the in-phase (real) portion of the impedance (no phase shift, i.e.

ohmic resistance of the bulk and paracellular pathway), while the imaginary axis quantifies the 90° out-of-phase (imaginary) contribution (i.e. double layer capacitance at electrode-solution interface and membrane capacitance) for each frequency. Monitoring parameters |Z|, *R* and *C* can be calculated from real and imaginary contributions according to the given equations.

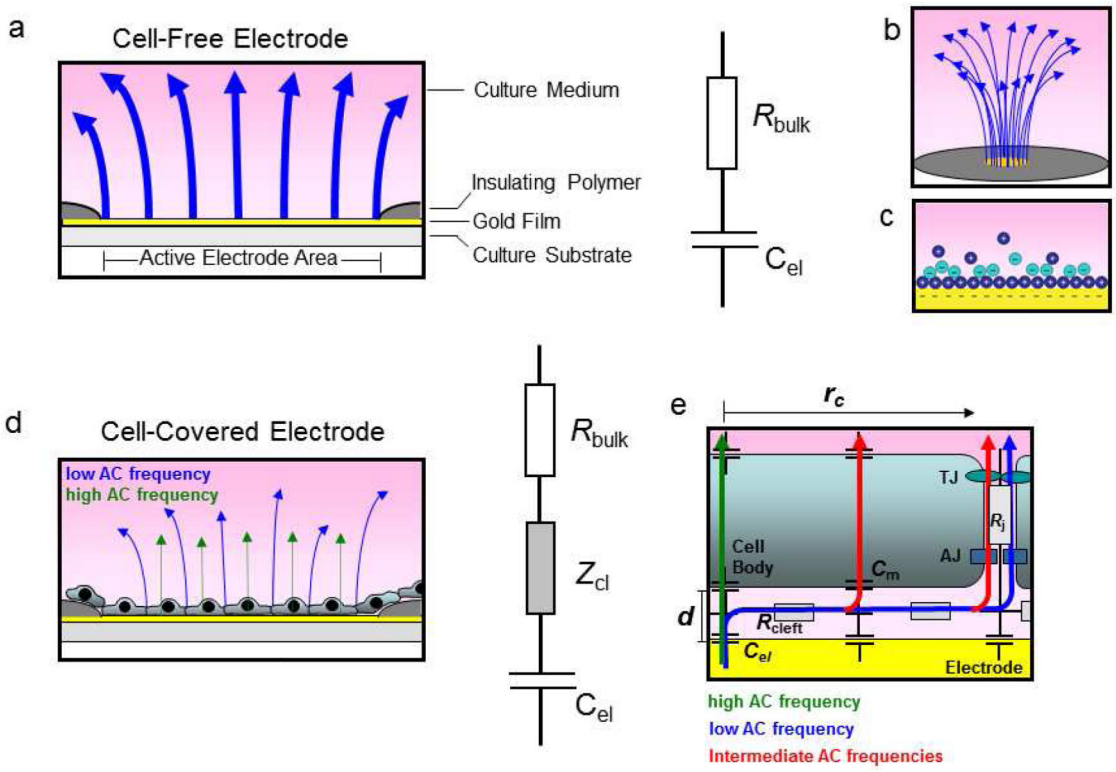

Fig. 4.

Schematic illustration of electrical behavior of a cell-free and cell-covered ECIS working electrode.**a** Schematic side view of a cell-free electrode and respective equivalent circuit presentation as resistor and capacitor in series. **b** Schematic presentation of electric compression of electric field lines (blue arrows) at the small opening of the working electrode. **c** Scheme of electrical double layer at a the electrode-solution interface. **d** Schematic side view of a cell-covered electrode, and respective equivalent circuit presentation which includes an additional impedance Z_{cl} that arises from the cell layer. **e** Schematic presentation of AC current flow at the cell layer-electrode junction. Depending on AC frequencies, two different limiting cases of current flow across a cell layer consisting of cells with the radius r_c in distance d above the electrode surface can be distinguished. At low frequencies the current takes the paracellular route (blue arrow) and takes up individual resistance contributions from the subcellular cleft (R_{cleft}) and the intercellular junctions (R_j). TJ: Tight junctions, AJ: Adherens junctions. At high frequencies the current couples capacitively across the membrane (green arrow). The impedance is dominated by the capacitance of the cell membrane (C_m). At intermediate frequencies current can take a varying combination of paracellular and transcellular routes (red arrows).

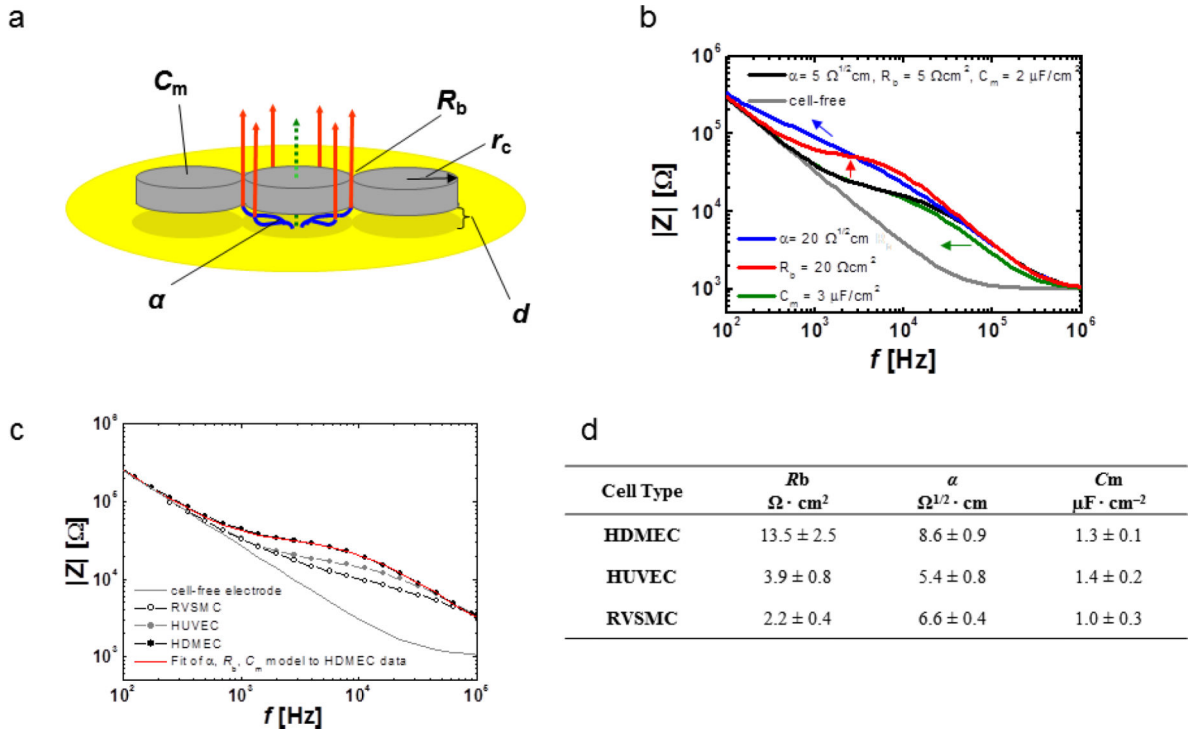

Cell Type	*R*b Ω · cm²	*α* Ω^1/2 · cm	*C*m µF · cm⁻²
HDMEC	13.5 ± 2.5	8.6 ± 0.9	1.3 ± 0.1
HUVEC	3.9 ± 0.8	5.4 ± 0.8	1.4 ± 0.2
RVSMC	2.2 ± 0.4	6.6 ± 0.4	1.0 ± 0.3

Fig. 5.

Analysis of confluent cell layers using the α, R_b and C_m model developed by Giaever and Keese. **a** Schematic representation of the model. Herein cell bodies are regarded as circular discs with a radius r_c and distance d from the electrode surface. Frequency dependent AC current flow (blue, red: paracellular; green: transcellular) is drawn unidirectionally for clarity. Impedance contributions from the cell layer can be separated into the three parameters α, R_b and C_m. **b** Illustration of changes in the three parameters α, R_b and C_m by simulated impedance spectra computed from the transfer function (software written by J. Wegener, University of Regensburg, 2010). From the initial settings (α = 5 $^{1/2}$cm, R_b = 5 cm^2, C_m = 2 µFcm^{-2}) (black trace) either α, R_b or C_m were independently changed to α = 20 Ω$^{1/2}$cm (blue trace) R_b = 20 Ωcm^2 (red trace) or C_m = 3 µFcm^{-2} (green trace). The grey curve represents the frequency dependent behavior of cell-free electrode. Arrows indicate direction of |Z| shift with increasing parameter value. **c** Experimental spectra from three different cell types: HDMEC, HUVEC (human umbilical vein endothelial cells) and RVSMC (rat vascular smooth muscle cells). The red curve represents the spectrum as obtained by least square error computations for suitable α, R_b and C_m combination that fit the experimental HDMEC data. **d** parameter values from fitting experimental data obtained from HDMEC, HUVEC and RVSMC using ECIS software.

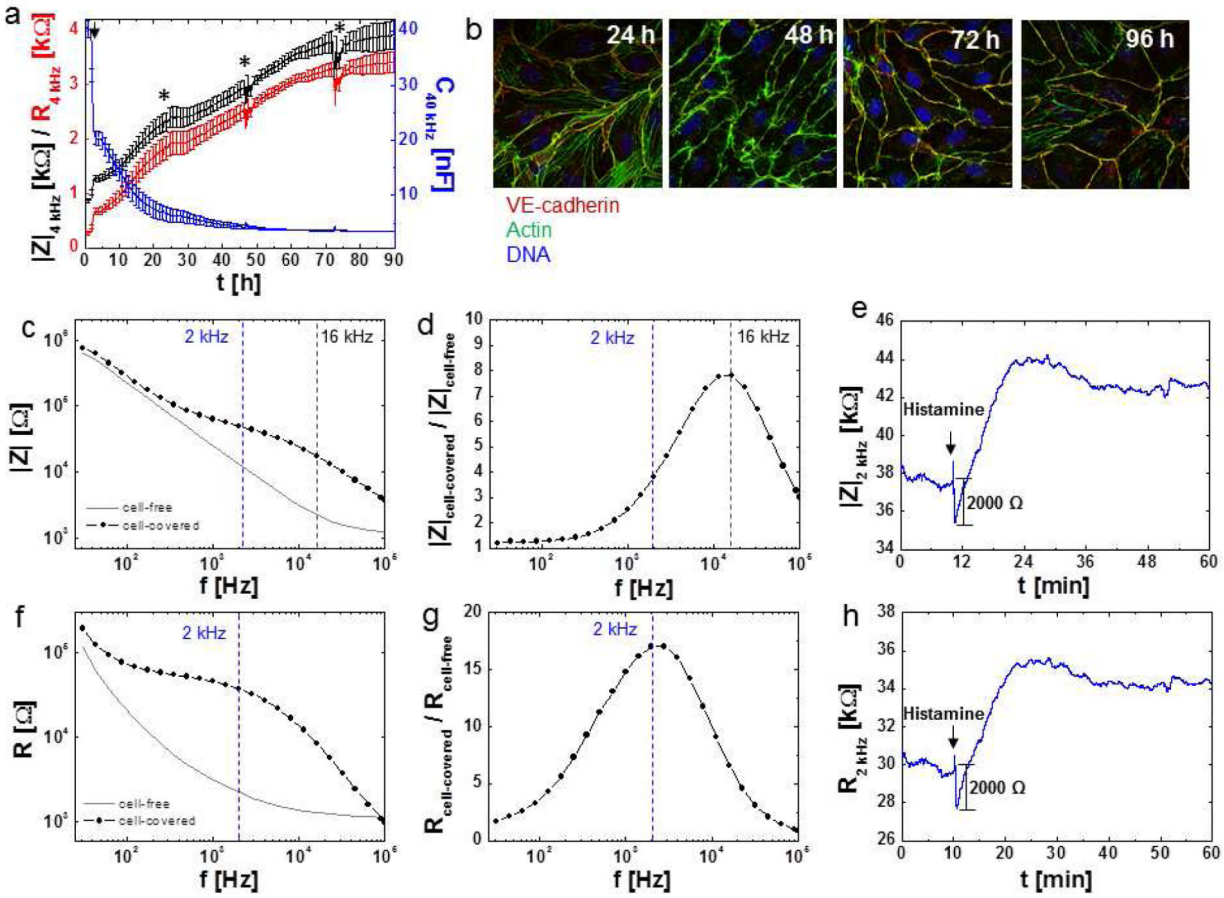

Fig. 6.

Monitoring parameters |Z|, *R* and *C*. **a** Time course of impedance magnitude |Z| (black curve) and resistance (*R*) (red curve) at 4 kHz (left y-axis) and capacitance (*C*) (blue curve) at 40 kHz (right y-axis) for 8W10E+ ECIS electrodes (average and *SD* of $N = 8$) inoculated with HDMEC cells (80, 000 cells per well), where indicated by an arrow. Culture medium was exchanged (50 %) at time points indicated with asterisks. **b** Confocal fluorescent micrographs of HDMEC 24, 48, 72 and 96 h after seeding on gelatin coated glass slides and stained for VE-cadherin (goat anti VE-cadherin, Alexa Fluor®594-labeled rabbit anti goat), actin (Alexa Fluor®488-labeled phalloidin) and DNA (Hoechst33342). **c – h** Monitoring parameters for endothelial barrier function. **c – e** Impedance magnitude |Z|, **f – h** resistance *R*. **c, f** frequency spectra of a cell-free and cell-covered (confluent HDMEC) 8W1E electrode for |Z| and *R*. **d, g** The ratio of the respective (|Z| or *R*) for a cell-covered electrode to a cell-free electrode is used to extract the monitoring frequency with maximum sensitivity. Maximum sensitivity to monitor changes at cell-cell junctions for a given cell type and a given electrode type (2 kHz in this case) are extracted from plotting $R_{\text{cell-covered}} / R_{\text{cell-free}}$ as a function of frequency. **e, h** Time course of |Z| (**e**) and *R* (**h**) at 2 kHz for the same confluent HDMEC cell layer grown on a 8W1E electrode in response to addition of 10 μM histamine (black arrows).

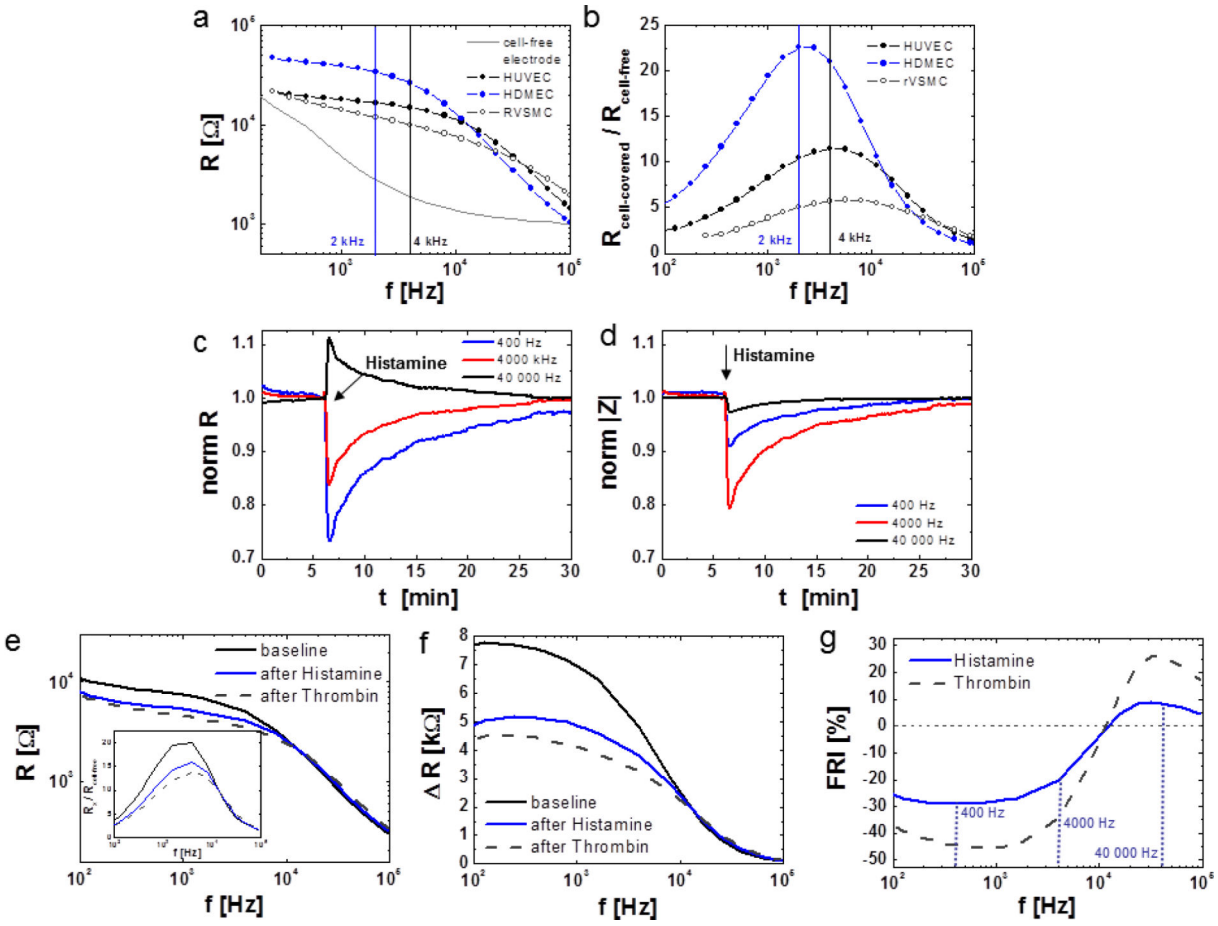

Fig. 7.

Cause and effect of changes in monitoring frequency on sensitivity. **a, b** Influence of cell type on ideal frequency for sensitive resistance monitoring. **a** Resistance spectra for HDMEC (blue), HUVEC and RVSMC grown on 8W1E electrodes. **b** Ratio of cell-covered to cell-free resistance ($R_{\text{cell-covered}}$ / $R_{\text{cell-free}}$) for each cell type as described in (a). **c and d** Influence of monitoring frequency on qualitative and quantitative changes in **c** *R* and **d** |Z| after stimulation of HDMEC on 8W10E+ with 10 μM histamine (arrow). **e** Resistance spectra for HDMEC under baseline conditions (black) and after stimulation with 10 μM histamine (blue) or 5 nM Thrombin (Thr, grey dotted curve). The inserted graph shows the Ratio of the cell layer to cell-free resistance (R_x / $R_{\text{cell-free}}$) for each condition *x*. **f** Frequency dependent difference in Resistance R (R_x – $R_{\text{cell-free}}$) for HDMEC under conditions *x* as described in **e**. **g** Frequency response index (FRI) for HDMEC cell layers upon histamine (blue) or thrombin (grey, dotted) stimulation. FRI has been defined as ($R_{(\text{max response})}$ − R_{start})/R_{start} × 100 [%]. Here, $R_{(\text{max response})}$ denotes the lowest resistance reached after agonist addition, R_{start} is the initial baseline resistance of the intact cell layer.

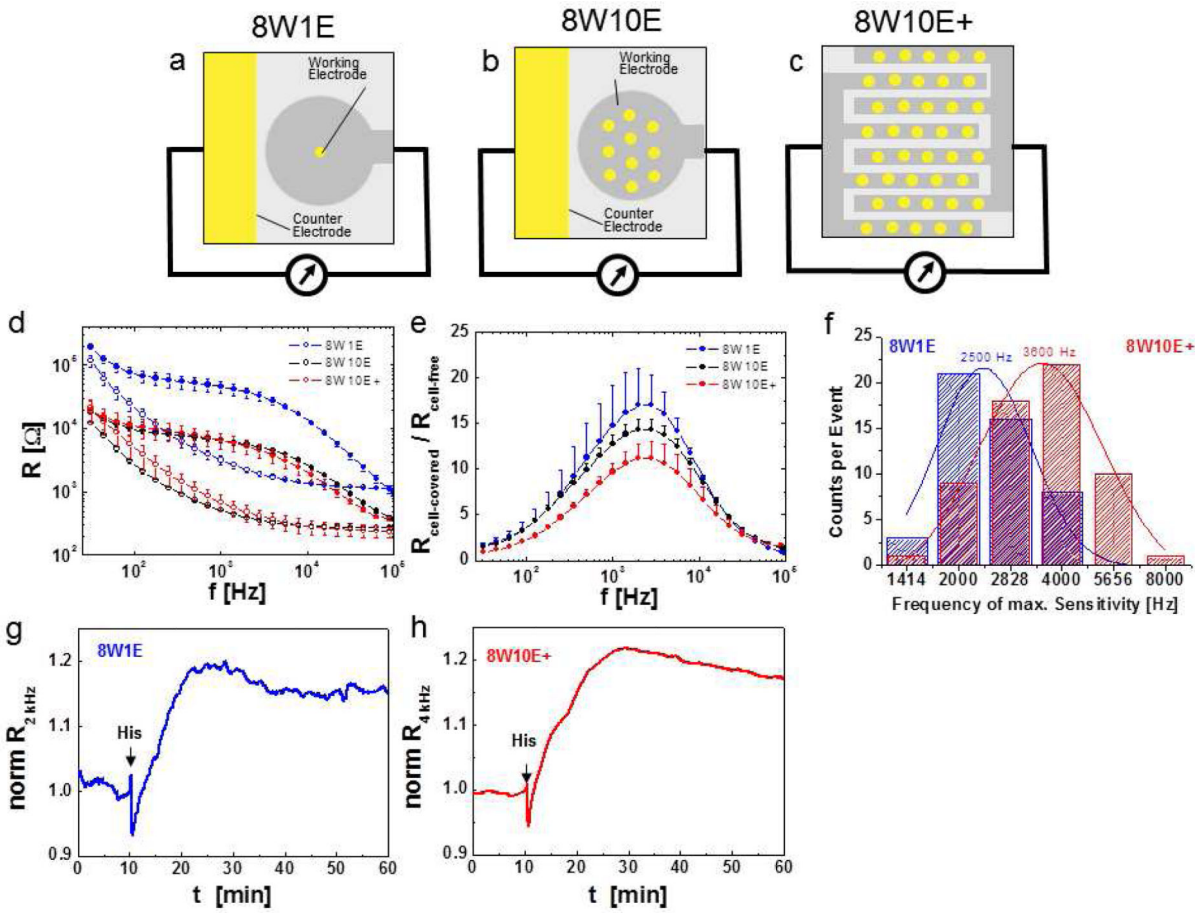

Fig. 8.

Electrode layouts influence sensitivity of ECIS measurements. **a – c** Schematic top view of coplanar electrode layouts of one chamber/well of **a** 8W1E (8 wells, 1 electrode/well), **b** 8W10E (8 wells, 10 electrodes/well) and **c** 8W10E+ (similar electrical behavior as 8W10E) arrays (yellow: gold electrode surfaces, grey: insulating polymer). **d** Resistance versus frequency spectra for 8W1E, 8W10E and 8W10E+ electrodes. The respective cell-free (traces with open circles) and cell-covered (confluent HDMEC; traces with closed circles) spectra (average and *SD* from 8 wells) are shown. **e** $R_{\text{cell-covered}} / R_{\text{cell-free}}$ as a function of frequency showing different sensitivities of different electrode layouts. **f** Distribution of maximum sensitivity frequency for 49 (on 8W1E), 61 (on 8W10E) individual confluent HDMEC cell layers (from different isolations and passage numbers) after 4 days of culture on either 8W1E (blue) or 8W10E+ (red) electrodes. **g, h** Resistance profiles of confluent HDMEC cell layers upon histamine stimulation (arrows) on **g** 8W1E and **h** 8W10E+ ECIS array, plotted as normalized resistance (normalized to resistance values before histamine addition) at their respective maximum sensitivity frequency.

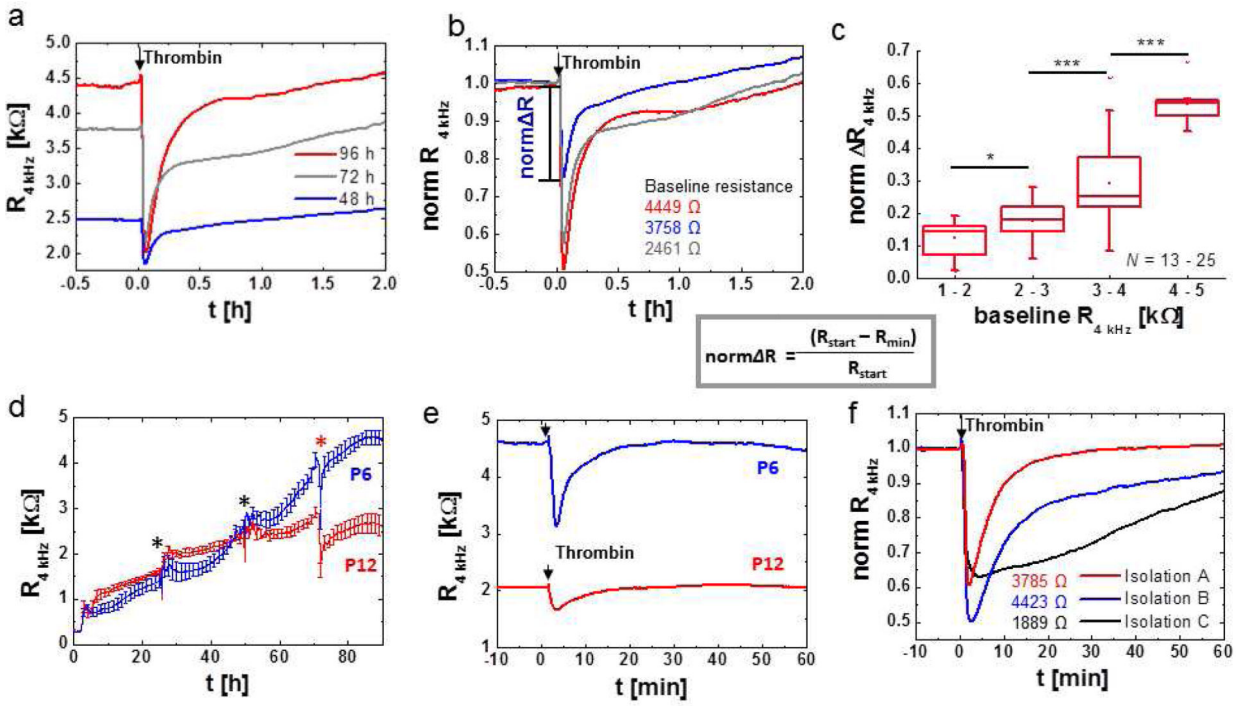

Fig. 9.

ECIS data presentation and influence of baseline resistance variability on signal intensity after GPCR stimulation. Presentation of resistance time courses of HDMEC on 8W10+ as **a** absolute resistance (*R*, in k) or **b** normalized resistance (norm *R*, dimensionless) at a monitoring frequency of 4 kHz. All absolute values were normalized to the last reading before the addition of 5 nM thrombin (arrow). Information on initial baseline resistance is lost when data are plotted as normalized values, if not explicitly documented within the figure or figure caption. Fig. **a** shows the influence of HDMEC culture time (48, 72 or 96 h) on initial cell layer resistance and signal intensity upon addition of 5 nM thrombin (arrow). **c** Statistical analysis on the influence of basal cell layer resistance on response intensity upon thrombin stimulation (5 nM). The normalized difference between baseline value (R_{start}) and the minimum resistance reached after thrombin addition (R_{min}) is plotted as a function of initial cell layer resistance and grouped in clusters of 1 – 2, 2 – 3, 3 – 4 and 4 – 5 k with each cluster representing data from $N = 13 – 25$ independent experiments. Note that data used for this analysis originate from HDMEC cell layers after at least 72h in culture. **d** – **f** Cell culture parameters that influence baseline resistance of endothelial cells and response intensity and kinetics to GPCR agonists. **d** Time course of resistance after inoculation of 8W10E+ ECIS electrodes with HDMEC cells at either passage P6 or P12 of the same isolation using the same cell number (80, 000 cells / well; average and *SD* from $N = 4$). **e,** Response of HDMEC cells at either passage P6 or P12 as from d to thrombin (5 nM) stimulation. **f,** Time course of resistance of 8W10E+ ECIS electrodes with HDMEC cells from the same passage number (P5) but from different isolations (A, B, C) after stimulation with 5 nM thrombin. Absolute resistance values of the respective cell layers under baseline conditions are included in the figure.

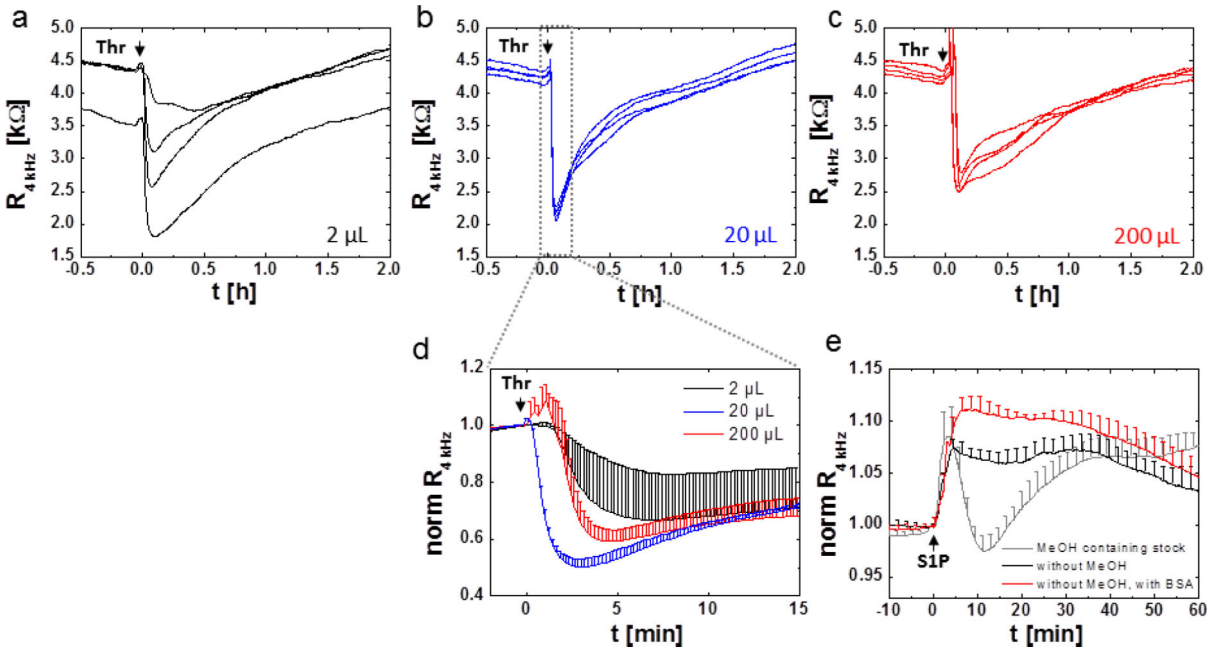

Fig. 10.

Influence of liquid handling during agonist addition and agonist preparation on signal intensity and reproducibility. **a** – **c** Color-coded response profiles of HDMEC cell layers grown on 8W10E+ electrodes after addition of thrombin using different fluid volumes for addition: **a** 2 µL of 200 × stock solution **b** 20 µL of 20 × stock solution **c** 200 µL of 2 × stock solution. A final concentration of 5 nM thrombin was reached in all conditions. The respective amount of medium is removed from the wells before the agonist is added to maintain a final volume of 400 µL. **d** Average and normalized response profiles of data from HDMEC layers shown in **a** – **c**. **e** Influence of different preparations of S1P working solutions on the response profiles of HDMEC cells upon stimulation with 1 µM S1P (arrows) (average and *SD* of $N = 4$). All S1P working solutions were prepared as a 20 × stock (20 µM) and added to reach a final well volume of 400 µL. Grey trace: S1P solution (1 mM) in methanol diluted (1:50) in low serum medium. Black trace: Methanol was evaporated from the S1P from the stock solution under a dry nitrogen stream and reconstituted in low serum medium with 5 min sonication. Red trace: Methanol was evaporated from the S1P stock solution as described above and reconstituted in HBSS with 0.03 mg/ml fatty acid-free BSA.